Design, Manufacture and Test of a Micro-Turbine Renewable Energy Combustor

Bahamin Bazooyar[1]

Hamidreza Gohari Darabkhani[2]*

Department of Design & Engineering, School of Creative Arts and Engineering (CAE), Staffordshire University, Stoke-on-Trent, ST4 2DE, United Kingdom

[1]Bahamin Bazooyar, Research Fellow in Turbulent Combustion (Bazooyar.bb@gmail.com)

[2,]*Corresponding author: Hamidreza Gohari Darabkhani, Professor of Low Carbon and Renewable Energy Systems

Email: h.g.darabkhani@staffs.ac.uk

Tel: +44 (0) 1782 292769

ABSTRACT: The ever-increasing demand on highly efficient decentralized power generation with low CO_2 emission has made microturbines for power generation in micro-combined heat and power (mCHP) generation systems popular when running on biofuels as a renewable source of energy. This document presents a state-of-the-art design, and optimization (in terms of design, performance and emission control) of a micro-turbine renewable energy combustor that fits into the existing Bladon 12kWe recuperated microturbine plenum while running on a range of biofuels as it can successfully provide the required power of the mCHP. Governing equations for in-depth analysis of the combustor consist of manufacturer empirical data to simulate system-level operation with respect to replacement of the fossil with biofuels. The Model developed and validated at company's ISO conditions confirms the output power of the new combustor fits the conventional system with slight eco-energy improvements. The modeling of the combustor in a complete microturbine assembly system is performed, then was utilized to further analysis of the microturbine with the designed combustor. The experimental results gave on average 46.7% electrical efficiency, 83.2% system efficiency, 12 kWe electrical power, and 90% recuperator effectiveness at nominal operating conditions of microturbine (MT). Sensitivity analyses evaluate changes in performance with respect to fuel phase (e.g., liquid or gaseous) and design variables (e.g., orientation, shape, and dimensions of combustor), leading to energy optimization of the unit. Experimental findings demonstrate that the combustor in microturbine can meet the target performance specifications of a company conventional diesel microturbine with significant savings. An objective function including both combustor and recuperator technical energy data is defined for finding the best ratio of fuel and air and their flow rates to find the most effective operating points for the operation of MT. Annual time series simulations completed for Coventry, West Midlands, United Kingdom indicate a new combustor can reduce operational costs of diesel

fuel combustor by 8%, 2%, 36%, and 25% when supplying bioethanol, DME, biogas, and NG, respectively. Annual operating time of the renewable microturbine combustor at rated capacity included an 11% reduction in exergy loss with biogas fuel relative to diesel fuel.

Keywords: Microturbine; Combustor; Design and Modelling; Biofuel; Carbon Neutrality.

1. Introduction

The rapid industrialization of the world intensifies the need for more efficient energy gensets. This necessitates the collaborative, industry-led research for novel combustors, new materials and sub-assembly designs leading to system integration, development, and testing, and finally evaluation of the integrated microturbine generators (MTG) for the carbon-free renewable energy sources, not only as they are a good replacement for the limited conventional petroleum resources in terms of energy production and efficiency but also as they form a reliable sustainable fuel supplies that could successfully solve the problems associated with the conventional petroleum energy sources by providing energy security and cleanliness of the atmosphere [1]. In the range of small to medium power generation frameworks, the industrial designs are stepping towards the improvement of already existing conversion systems, the direction of distributed energy systems, and the use of renewable energy technology in the development of heat and power combined systems [2], three of which could be considered in the design of micro-turbine in the power integrated frameworks, thereby increasing the energy efficiency and lowering the electricity production costs significantly [3]. This multipurpose integrated energy ambition brings up the research and development for design and development of novel integrated microturbine gensets that can be successfully run on biofuels, particularly for the operation in remote locations under off-design operations where the demand for energy is oscillating and transportation of it challenging such as Sub-Saharan Africa with 600 million people who do not have a connection to

148 the electricity grid with only seven countries having electricity rates over 50% even in 21st Century
149 [4]. Many micro-turbine designers in the Europe Network Association (ENA) such as European
150 Turbine Network (ETN) and Bladon microturbine in the United Kingdom have now strongly
151 supported the research agenda for design and development of micro-turbines running on the
152 renewable fuels to decarbonize the gas network moving according to the government policies and
153 outlooks.
154 Despite other combined heat and power technologies, the microturbines have superior fuel
155 flexibility that could successfully burn fuels with a high level of contaminants and low calorific
156 fuels [5,6]. The choice of fuel is very decisive in the operation of the combustor in the microturbine
157 (MT) integrated energy system. For low heating value gaseous fuels, the main attention in the
158 design of microturbine is to improve the combustor. The microturbine combustors usually operate
159 with a partially premixed swirling flame where the lean air-fuel mixture is fed with hot air at
160 different stages along the chamber [7]. MT combustors should provide a high air/gas mixing
161 quality with sufficient residence time needed for the low calorific fuels to complete the combustion
162 as well as uniform outlet temperature distribution [8]. MT combustors also control the micro
163 turbine's work output, the level of the emissions and the turbine operating temperature [9].
164 Accurate design of the combustor could mitigate the problems of autoignition, dynamic or static
165 instability, keep temperature profiles, NOx and CO emissions within allowable limits, curtail the
166 flame encroachment to the rim of the flame holder, and promise the long life of the MT
167 components. Of particular interests in combustor design are the swirler type, nozzle guide vanes,
168 liner, casting and end-wall platform. These parts of the combustor are usually subjected to a very
169 highly reactive hot turbulent flow field, thereby are being exposed to erosion, thermal stress,
170 leakage, thermo-mechanical damages [10] and corrosive emissions [11]. The non-uniformities,

chaotic, and harsh flow characteristic impact the flow development and temperature on the solid components. The lifetime of microturbine components including blades, and combustor itself are extremely sensitive to the temperature and steep temperature gradients [12–14]. Other challenges in the design of the small combustors are sufficient residence time for reactants and the heat loss due to the high ratio of surface to volume, especially when small burning fuel is considered. In the case of MT combustors, these potential problems would be extremely serious due to the compactness and small thickness of combustor walls making it necessary to be carefully managed and considered in design of a novel combustor. The design of air staging technique [15], swirl intensity [16], spray characteristics [17], and equivalence ratio [18] is necessary for proper combustion of the whatever the fuel and to maintain the emission standards, performance, and operability over the entire range of energy desires [19]. All the above considerations make it necessary to carefully redesign the new combustor parts including swirler, nozzle, liner and casing for any new fuels or operational objectives.

In response to the off-land design perspectives, where energy hubs are faraway, the demand for the energy is oscillating, and transportations of fossil fuel is challenging, the design of combustor in a micro CHP energy integrated system that could efficiently operate with a local residential renewable fuel over a wide range of energy demands turns out to be interesting [20]. Conventionally, the use of liquid fuels such as diesel was prevalent in small scale energy gensets as they have high energy contents in specific volume. As the emission regulations continue to tighten, and the available energy supply becomes insecure, the use of gaseous and biofuels has been popularized as an invaluable outlooks in design and analyze of microturbines under various scenarios as it requires fewer sites visits, leads to the longer life of the microturbine components, has low noise and vibration, and could successfully support the multi-mode operation while it has

194 a superior compliance with the emission standards. The design of the combustor for renewable
195 fuels requires analyzing the flow paths within a gas turbine and an extensive literature review to
196 find experimental combustor models that have been previously used and could successfully
197 describe the long-term operation of the turbine under a variety of operational points. Upon
198 completion of the design, modifications were made to the combustor for the installation of it in the
199 microturbine genset. The overall design of microturbine was then benchmarked through velocity,
200 pressure, temperature, turbulence measurements, the material, and manufacturing [21].
201 The design and development of both small stationery and automotive gas-turbines began on
202 1950′s which now eventuate into the two types of today's modern MGT [22]. In developing the
203 microturbine for power generation, considerable attention has been paid to improving the
204 combustor. The choice of appropriate fuel nozzle, swirler, and a flame holder with enough air
205 staging holes could lead to efficient mixing of the fuel and air and efficient combustion at different
206 stages within a short period of time. The use of biofuels may put some limitations on the long-term
207 operation of the MT (e.g., clogging in atomizer orifice, more CO emissions, turbine malfunction
208 [23–26], reduction of static thrust [27], and vibration [28]), making it necessary to consider
209 stringent revisions or even redesign in the precedent combustors that already operating well in the
210 MT assemblies. Laranci et al. [29] have shown that in the case of biomass-derived fuels the
211 occurrence of high-temperature creep phenomena affects the liner walls leading to the high
212 temperature oxidation damage. Chiong et al. [30] have stated that in the case of renewable fuels
213 “Modified fuel delivery system with the heating capability and improved atomization technique
214 can be applied to overcome the limitations of the fuels”. Due to such these limitation in the use of
215 biomass-derived fuels, the trend of using third-generation fuels in MT is currently moving to the
216 biomass conversion and production of biofuels. However, the application of these fuels is also not

devoid of limitations and these fuels impose some modification to the combustion systems and components of the MT. In the recent state-of-the-art review, Ibrahim I. Enagi [31] summarized that the novel combustion technologies including colorless distribution combustion, moderate or intensive low oxygen combustion (MILOC), high-temperature air combustion, and catalytic combustion are needed to enhance the combustion performance and stability of lower grade biofuels in the combustors of MT. Another but equally efficient approach is to design a new combustor with specific fuel injection and air aerodynamic. Many studies could be found in the literature that aims to design new combustors. They, however, benefit from the high-grade petroleum fuels with high energy density. Enagi et al. [32] have designed an MGT combustor for LPG fuel and improve the combustor fundamental characteristics such as low outlet temperature and CO emission. They have reported that the chamber geometry and strategy of air staging including the primary, secondary, and dilution holes and dimensions could help the designers achieve the optimal operation of the combustor. Talluri et al. [2] have presented an innovative design of the Tesla micro-expender which takes all the assembled components (i.e., plenum chamber, diffuser, stator, the rotor and etc) together rather than consider them separately in the design perspectives. They have shown that microturbine thermal to mechanical power transmission is more efficient at low mass flow rates and inlet pressures. The inlet temperature was reported to have a negligible influence on the turbine performance. Delatin et al. [33] have applied the syngas fuel in a pressurized microturbine-like combustor and experimentally analyzed the temperature profiles, flame shape and position, emissions, and operability issues. Although the level of CO and NO_X are low, the temperature profiles did not surpass that of the natural gas, and the operability issues including flash-back, autoignition, combustion dynamic instabilities were not observed, they have pointed out that the full test of the MT assembly is needed to rest assured

240 that the operation of this fuel in the MT is safe. In another study [34] , they have reiterated that
241 some modifications to the combustor may be needed, especially to the dilution holes, to maintain
242 the optimum operations of the combustor. Waitz et al. [35] have designed a hydrogen-air micro
243 combustor for the microturbine engines. The wide flammability range of hydrogen-air mixture
244 enables the occurrence of the combustion at lean conditions, thereby obviating the need for the
245 dilution, combustor cooling, and strong body material. MacDonald and Rodgers [36] have
246 designed a 7.5 kW natural gas-fired based ceramic radial flow turbine with a ceramic combustor,
247 and a compact ceramic fixed-boundary high effectiveness recuperator. Their new turbine could
248 provide the energy requirement of an average house and could be successfully coupled with a solid
249 oxide fuel cell (SOFC). However, they promulgated that any viable ceramic microturbine
250 assembly larger than their design should be carefully benchmarked to attain the efficiencies of
251 more than 40%. Fantozzi et al. [37] have stated that in the combustion of syngas in MT the hotspots
252 are reduced and flame stabilization occurs closer to the fuel nozzle, all these make it necessary for
253 the design of a specific combustor for this hybrid flames, and any new fuel in renewable
254 technology. The same changes should be observed in the case of biogas which is like the syngas a
255 combination of a combustible CH_4 with an inert CO_2 gas. The discussion above makes this point
256 clear that the generalization of the combustor for any new fuel may deteriorate the normal
257 operation of the combustor and it could even detrimental for long term operation of the MT,
258 reputation, and prestige of the design companies.
259 Structural dimensions, combustion performance, and emission characteristics are important
260 parametric design variables in the design of combustors for gas turbines. The need for more inlet
261 velocities, temperatures, and equivalence ratio have increased the thrust weight ratio of gas in the
262 turbine, making it extremely difficult to reduce the pollutant emissions while it widens the stable

combustion range and extent of the service life of the combustor [38]. There are different types of combustor that have designed so far to meet the emission standards and to keep the stable combustion range. The trapped-vortex combustors have shown great potential for conventional fuels in MT [39] and could be considered for the biofuels.

Three design criteria are of crucial importance in the microturbine combustor technologies. First, the trapped vortex formed by recirculation of the combustion product should be reinforced using suitable fuel and air injection [40] to widen the stable combustion range [41]. Second, superior sustainable combustion performance should be attained by preheating combustion by-products via recirculation materials. Third, pollutant formation (NO_X and smoke emissions) should be controlled through the staging of air intro the combustor [42]. The novel design of the combustors is to increase the overall efficiency, thrust-to-weight ratio, and to reduce the weight and pressure loss. This design aims to adapt and merge the combustor parts with the case components of the gas turbine. The core part of the combustor is a perforated annular metallic annulus. The central part of the combustor is a key factor affecting the rate of air to fuel mixing [43] and the level of emissions [44]. It is of predominant importance that the fuel and air mixed quickly and burned efficiently within a short residence time. There is a high intricate relationship among the flow and combustion characteristics within the parts of the combustors, making it necessary to carefully choose the rate of the air and fuel to any designed combustors [45]. The shape and dimensions of the fuel nozzle and swirler pronouncedly influence the high acceleration and high-turbulence of the combustion environment, as a result, flame length. The spatial mass fraction should happen far from the combustor rim to put up the high thermal stress on the walls, thereby promising a long-term operation of the combustors. The strategy of air staging should also be managed to control any unheralded increase in the combustor wall temperatures as well as NO_X emissions. The turbine

inlet temperature (TIT) which is combustor outlet temperature could damage the turbine vanes and stator if not carefully controlled [46].

The micro-gas turbine performance (emissions, efficiency and energy destruction) correlates with the deviations of any new biofuels properties from those of the baseline fuels [47]. The main objective of the paper is the design and manufacturing of a 12kWe combustorto effectively operate with a range of biofuels and therefore provide the energy requirement of the MT shaft. This new combustor could target the plan and strategy of the UK to achieve its goals in off-land design application. The UK government aspires to be at the forefront of supporting the development of new technologies that make cost-effective use of existing resources while enabling the emergence of low carbon technology. The efficient utilization of renewable energy is a must to achieve the overall goals set by the government which has set a target to increase heating from renewables from 5% to 26% (over 60TWh per year). The control and optimization of the combustor require prior determination of feedstock, the required stoichiometric conditions, and control of the pollutants. The design of the real combustors is still based largely on a long-term experience for any new fuel [48]. The proposed 12 kW biogas micro turbine generator (MTG) product aims to promote increased use of biofuels whilst reducing operational and maintenance costs for decentralized power generators due to the high utilization and extended service life and maintenance intervals offered by the biofuel driven MTG. This study is categorized into four main parts which aims to firstly provide the conceptual and preliminary design of a 12 kWe combustor, secondly, perform CFD modeling of the high-pressure micro-combustor burner, thirdly improve the efficiency and emission control of the combustor with a degree of fuel flexibility, fourthly and finally performing energy-exergy-economy analysis of the 12 kW MTG with the designed combustor.

The focus on renewable bioenergy makes the product to capitalize on the emerging use of the fuel in many nations with poor or unreliable connectivity to the grid such as in Sub-Saharan Africa (SSA) and southeast Asia. The novel work undertaken by the paper will be the development of a gas combustor which makes use of the inherent fuel flexibility of a microturbine engine to enable the burning of different biofuels with no fundamental change to the core microturbine generator. To date, no such microscale Closed Cycle Gas Turbine (CCGT) system or microturbine system operates with these fuels due to their low calorific value and impurities, without impacting its current combustion, the economic and technical challenges of micro-scale heat-to-power systems, and micro-turbine performance. The performance that needs maintaining includes; low NOx emissions, the combustor's ability to light and burn efficiently throughout the cycle and achieving the required life. This paper will also briefly elaborate on what biofuel pre-processing plant will be needed, prior to the microturbine, and its associated costs, and another study on the market analysis and cost modeling of the bio-fuel distribution system. This will allow the feasibility of the entire process of MTG design and development to be assessed and understood. At the 12 kWe power generation, the design of renewable energy technology combustor is the first of its kind.

2. Material and method

2.1 Bladon micro Turbine

Bladon microturbine as a MTG manufacturer is a pioneer company in the design and development of micro turbines for telecom power towers by launching the world’s first 12kW practical gensets. The company now targets the use of biofuels in MT generators to move along the UK policy to reach the 2050 UK net zero carbon emission. The use of biofuel-based fuels on a state-of-the-art design targets the UK contribution in Paris agreement.

2.2 Microturbine combustor

In this part, the design strategy of the combustor is presented. The step by step procedure of the combustor design is shown in **Fig 1** which is a standard procedure for design of the vortex combustors. It includes 1) the calculation of the combustion stoichiometry and required fuel to meet the 12 kW output power, 2) the design of the combustor geometry, swirler, and fuel nozzle, 3) CFD simulation of the combustor for determination of gaseous emissions, material design, thermal stress at the walls, analysis of combustor flexibility to run at different operating points and improvements, if any, 4) and to test the designed combustor under the real MT operating condition, 5) and finally after assuring the accuracy of modeling approach, to test the combustor with different biofuels.

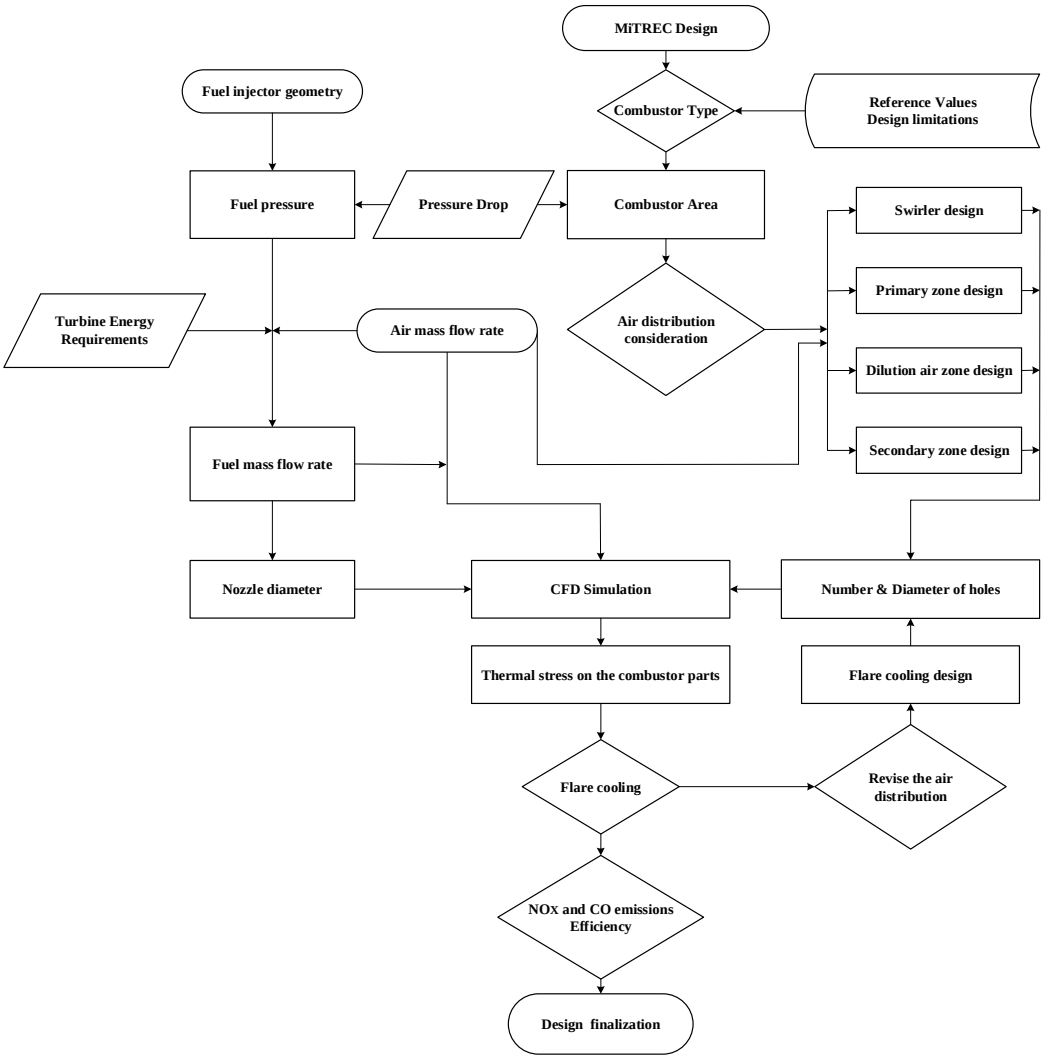

Fig 1 Design procedure for the MiTREC.

The design includes the following considerations:

1) The combustor locates on a microturbine plenum which contains recuperated air.
2) A vortex combustor made of the stainless steel 310S with 3mm thickness is considered for burning the biofuels in the MT.
3) A radial swirler with 10 vanes are deemed to stabilize the flame in the combustor and promise sustainable combustion.

4) The air staging technique at three steps (primary, secondary and dilution) through the liner is considered for the combustor to control the NO_X, promise uniform combustion, and to obtain the required outlet temperature
5) The residence time from the inlet of the mixing duct to the combustion chamber is designed to coincide with the ignition delay time of the fuel mixtures.
6) The distribution of air was deemed 7% for swirl, 5% for the head cooling, 8% for the primary, 18% for the secondary, and 62% for dilution. The fuel mass flow rates for biofuels were obtained from Aspen Plus software to meet the requirement of the company in terms of TIT. Table 1 gives the quantities of air and fuel mass flow rates.
7) The fuel injector is considered in 1.5 mm diameter with five passages, through one of which the fuel is sprayed coaxially, and with the other four fuel is sprayed with 45^o inclination angle. The design and location of the nozzle in the combustor is of crucial importance to avoid any flashback, entrainment, flame blow off-especially in the case of diluted biofuels (i.e., biogas) and those having low ignition temperature with high flame speed. For this combustor, the design and position of both swirler and nozzle were set after the optimization process.
8) The combustor was revamped to operate normally and satisfy the energy requirement of the MT. The fuel flexibility for the combustor was also taken into account so that it operates well with four different biofuels: biodiesel, biogas, dimethyl ether, and bioethanol.

Fig 2 demonstrates the schematic of the designed microturbine renewable energy combustor.

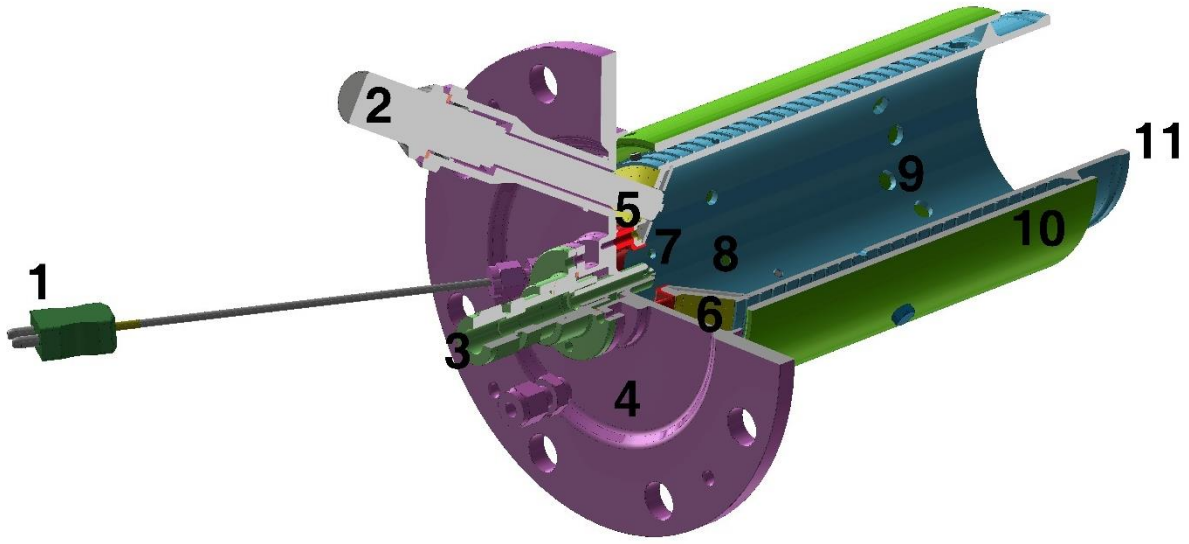

Fig 2 Combustor layout (1. K-type Thermocouple, (T31: combustor inlet air temperature 2. igniter 3. fuel injector main inlet 4. combustor end cover 5. swirler 6. head cooling sleeve 7. primary holes 8. secondary holes 9. dilution holes 10. casing 11. liner

2.3 CFD analysis

2.3.1 Computational domain and CFD models

The numerical simulation is to implement the design of the combustor ensuring flame stability, efficient combustion, fuel flexibility, optimization and finalization of the combustors. The CFD simulation includes the drawing the combustor with SOLIDWORKS 2018 software and defining a computational domain therein for the occurrence of the combustion, determining the boundary conditions, choosing governing equations, appropriate combustion and turbulence models with the required degree of comprehensiveness, solving the model equations, verification, validation and finally post-processing the results which all were accommodated using Ansys 19.2.

The continuity, Navier-Stokes, energy, and equations corresponding to transport and reaction of species are solved in the computational domain. To this end, the turbulence is modeled by $k-w$ shear stress transport (SST) [49] and turbulent flame chemistry is estimated as 32 counter-flow diffusion flame with 64 grid points [50]. The Flamelet Concept is exploited to handle chemistry/turbulence interactions. The discrete ordinates (DO) model [51] was employed to solve the radiative transfer equation in the energy balance source term to deal with the gas heat radiation to the combustor walls and environment. The contribution from the liquids is also considered in the transfer of heat by radiation in the combustor. The combustion chemistry for different biofuels includes Pei et al. [52] for diesel, Westbrook et al. [53] for biodiesel, Smith et al. [54] for natural and biogas, Fischer et al. [55] for DME, Marinov et al. [56] for bioethanol for handling the formation and destruction of species. Since the chemical time-scale associated with nitrogen oxides is much larger than fluid mixing time-scale, Flamelet Concept could not show the evolution of nitrogen oxides [57,58]. The thermal and prompt mechanisms were considered for NO_X using extended Zeldovich and De Soete formulations [59]. The concentrations of O and OH radicals were estimated using equilibrium and partial-equilibrium, respectively [60]. The interaction of NO_X with turbulence was obtained using a beta function probability function.

According the extended Zeldovich mechanism, the reaction rate (W_t, $\mathrm{mol/(m^3.s)}$) for thermal NO is:

$$W_t = \left(4.524 \times 10^{13.5}\,\mathrm{m^{1.5}}/\left(\mathrm{mol^{0.5}}.\,\mathrm{s}\right)\right)\exp\left(\frac{-69{,}466\,\mathrm{K}}{T}\right)c_{O_2}^{0.5}\,c_{N_2}\left(\frac{T}{1\,\mathrm{K}}\right)^{0.5} \quad (1)$$

where c_{N_2} is the nitrogen molar concentration, g/mol, and r is the mean density of the mixture, $\mathrm{gr/m^3}$.

The rate of prompt NO formation from the fuels is estimated using one step mechanism. The reaction rate (W_p, $mol/(m^3.s)$) for prompt NO is obtained from:

$$W_p = (6.4' 10^6 s^{-1}) \exp\left(\frac{-36{,}510\ K}{T}\right) c_{O_2}^{0.5} c_{N_2} c_{Fuel} \left(\frac{M_{mix}}{r}\right)^{1.5} \quad (2)$$

where M_{mix} denotes the mean molar mass of the combustion mixture, g/mol , and r indicates the mean density of the combustion, g/m^3.

In the case of liquid fuel (i.e., bioethanol, petrodiesel, and biodiesel), the liquid atomization, dispersion, and movement of particles have been added into the modelling using Lagrangian stochastic. In this work, linearized instability sheet atomization (LISA) represented by Senecal et al. [61] was considered for spray modelling and diameter determination of liquid droplets (i.e., liquid atomization). For spray dispersion, Lagrange equation was solved within the model to give the trajectory equation of individual particles. The random walk stochastic tracking was employed to model the dispersion of particles due to the turbulence. The cloud model was utilized for modelling of the statistical evolution of a cloud about a mean trajectory. Particle concentration om the cloud was considered in the model using Gaussian probability density function (PDF) [62]. Appropriate mathematical equations for thermal capacities, conductivities, dynamic viscosities of combustion species and fuel are considered [63]. The absorption coefficient of radiant species (e.g., O_2, N_2, NO, H_2O, fuel, CO_2 and CO) are also expressed using as a polynomial function of temperature [64–66].

2.3.2 Boundary conditions and operating conditions

The boundary conditions are defined for fuel, swirl, head cooling, and staging airs (primary, secondary and dilution) inlets, and a pressure outlet. The mass flow rates, pressures, and turbulence characteristics are specified at the boundaries. For walls, stainless steel S310 material with a

thickness of 0.89 mm, density 8030 kg, thermal conductivity of 16.27 W/m K, and specific heat of 502.48 J/kg K is considered. The conjugate heat transfer across the wall was accounted for using convection as well as conduction by solid in CFD solver.

Table 1 Boundary conditions of the combustor

Streams	**Temperature [K]**	**Mass flow rate [gr/s]**	Fuel formula
Fuel_inlet			
Biogas	292	3.16	
57%CH_4+42%CO_2			
Natural gas	292	1.085	CH_4
Biodiesel	298	1.29	$C_{18}H_{34}O_2$
Bioethanol	298	1.82	C_2H_5OH
Dimethyl-ether	298	1.678	C_2H_6O
Diesel	298	0.983	C_2H_6+ C_2H_6
Air_inlets			
Swirl	920	17.92	
20.9%O_2+79.1%N_2			
Headcooling	920	6.4	
Primary	920	8.342	
Secondary	920	21.451	
Dilution	920	73.887	
Outlet	1217	[129 131]	

2.3.3 CFD solver and verification

The steady-state finite volume solver including a simple scheme for pressure-velocity coupling, the standard for pressure, and least-squares cell-based with second-order upwind was chosen to find the solution in the domain. The convergence was achieved by monitoring the results at the outlet plane and residual of the differential equations, both of which lead to satisfactorily constant values upon the competition of the solution. The CFD verification involves the grid-independency analysis by comparing the numerical results obtained by using a different number of grids. The number of grids of approximately 1.2, 3.2, 5.3, 8.4, 10.5, 12.8, 18 and 30 million. No significant variations (below 5%) are achieved in results in terms of the distribution of temperature, pressure and species concentration between the structured grids quantities of approximately 8 to 18 million. The domain with 12.8 million meshes is used to analyze the results.

2.3.4 post-processing method.

For the analysis of the combustor, the coordinates are normalized to non-dimensional axial and radial values (i.e., z/L, r/R). The z/L= 0.0662, 0.1589 and 0.3939 account for the position of primary, secondary, and dilution holes respectively. For the scalar variables, the area-weighted average quantities are used for the post-processing of the results as follows:

$$f_{ave} = \frac{\sum_{i=1}^{n} f_i A_i}{\sum_{i=1}^{n} A_i} \quad (3)$$

The composition of gaseous species (e.g., fuels, emissions, and free radicals) are averaged by area-weighted-volumetric concentrations. The values (CO), (fuel), and (NO_X) are calculated on the base of 15% percent oxygen. The combustion efficiency is calculated by determining the heat loss at the combustor outlet via the incomplete combustion products [67].

$$h = 1 - \frac{Q_{CO}[CO] + Q_{fuel}[fuel]}{Q_{fuel}[fuel]\phi} \times 100\% \quad (4)$$

in which Q_{CO}=282 kJ/mol and Q_{CH4}= 794 kJ/mol. The $[fuel]\phi$ denotes the average volumetric concentration of methane in combustor when there is no combustion. It is equal to $[CO_2]+[CO]+[fuel]$ at the liner outlet when the combustion takes place.

The calculated h, could be also similarly estimated from:

$$h = \frac{[CO_2] + 0.645[CO]}{[CO_2] + [CO] + [CH_4]} \times 100\% \quad (5)$$

To represent pressure loss, a new parameter, namely pressure loss factor, is defined according to the following formula:

$$s = \frac{P_e}{P_i} \times 100\% = \left(1 - \frac{\Delta P}{P_i}\right) \times 100\% \quad (6)$$

where P_i and P_e indicate the inlet and outlet pressure, which is the area weighted average, and ΔP deltaP represents the differential pressure between the P_i and P_e.

The outlet temperature distribution exit was also calculated by the following formula [68]:

$$OTDF = \frac{T_{e,\max} - T_{e,ave}}{T_{e,ave} - T_k} \quad (7)$$

In above equation, T_k, $T_{e,\max}$, and $T_{e,ave}$ represent the spatial ,outlet maximum, and average temperature, respectively.

2.4 Experimentation

The combustor was manufactured in Bladon MT Ltd and tested in an experimental rig in Coventry, Midland, the United Kingdom in the company premise, Proving Factory. Fig 3 shows the picture of the manufactured combustor and its gaseous nozzle.

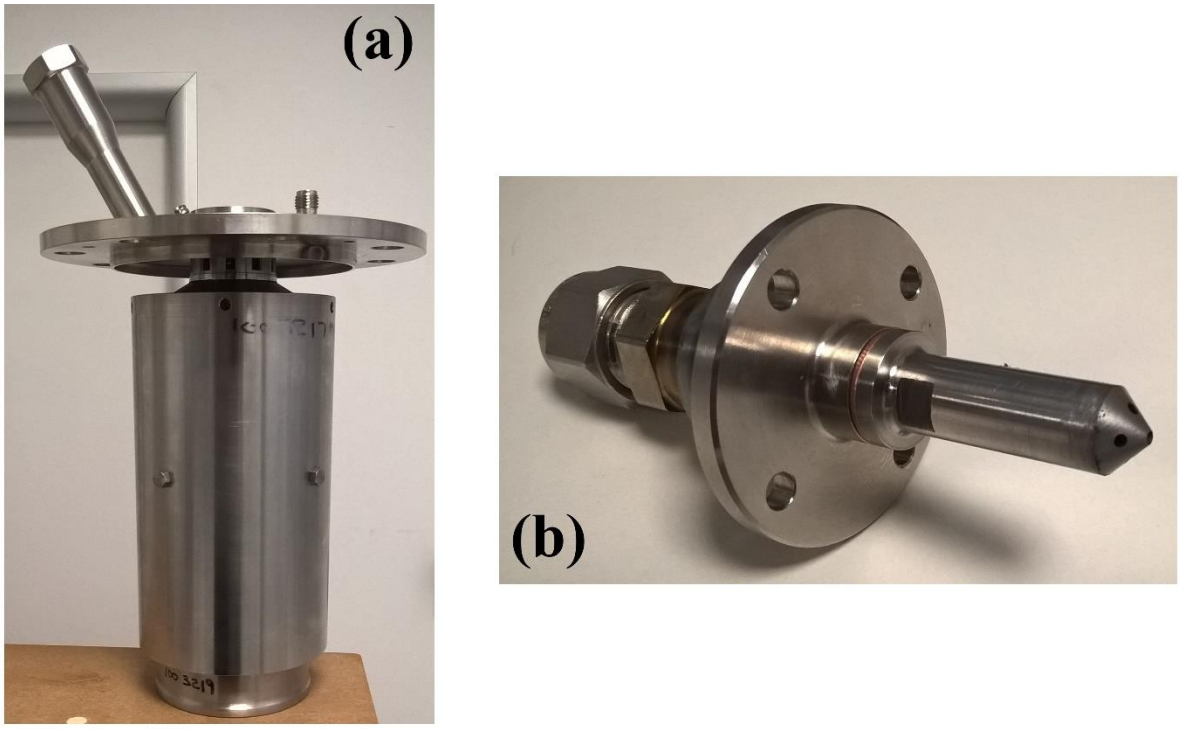

Fig 3 the full size of combustor prototype: (a) swirler, liner and casing, etc (b) fuel injection system

483

484 *2.4.1 Combustor characteristics*

485 The physical characteristics and geometrical features including effective area, inner and outer
486 diameters, radial and traverse direction and swirler effective area of the manufactured combustor
487 were determined by the Loughborough University. **Fig 4** includes the characteristics of the
488 combustor manufactured in the Bladon MT.

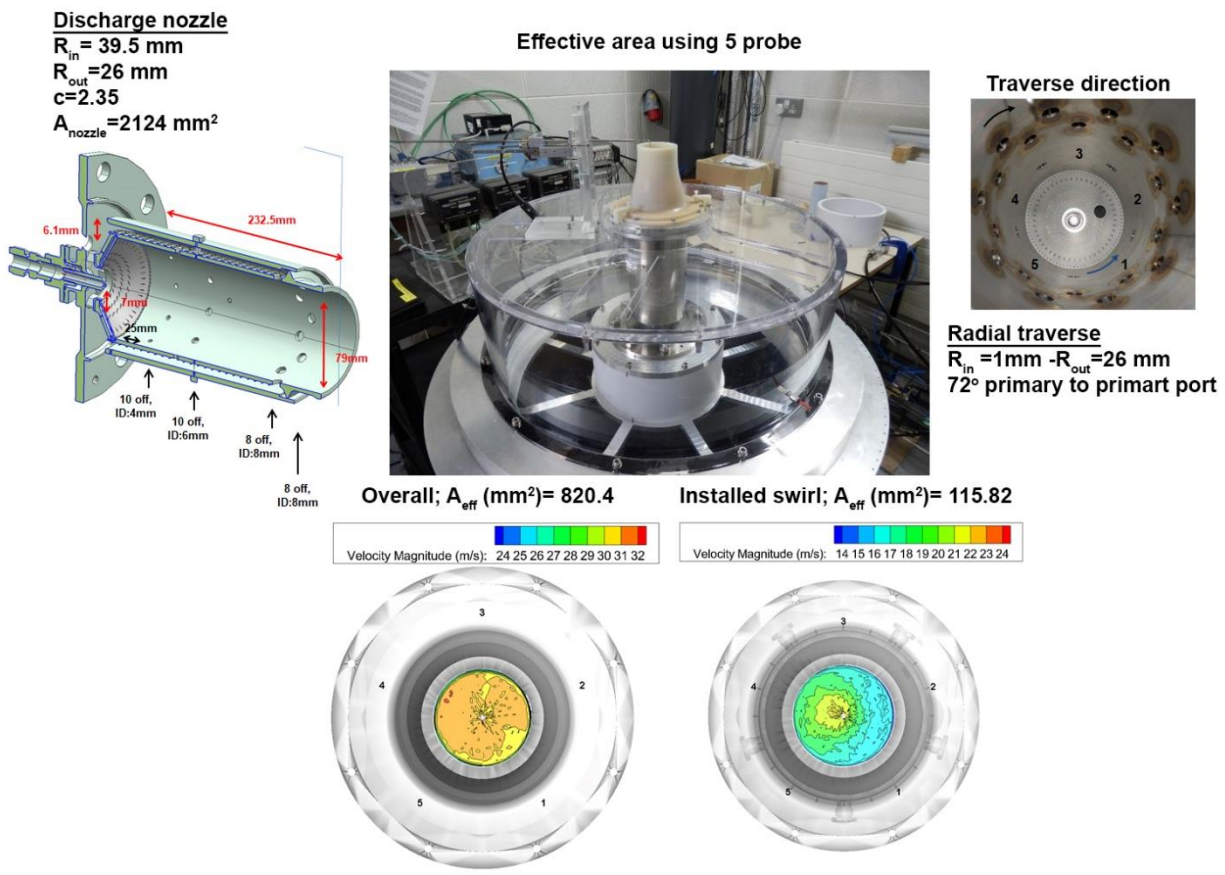

Fig 4 the combustor characteristics determined by Loughborough University

489

490 *2.4.2 Experimental setup*

491 An experimental rig is used to validate the CFD model and to compare the numerical methods
492 with measurements.

493 **Fig 5** depicts the experimental rig and the measurement devices. The fuel (including methane
494 and carbon dioxide) is obtained from two containers and mixed before entering the combustor.
495 The air is supplied from blower to a storage tank, then is compressed and heated to mimic the
496 conditions of the microturbine plenum recuperated air. The air storage tank mitigates the air
497 pressure fluctuation. Air filter and a mass flow meter are also in the air pipelines to remove the

impurities as well as provide a specific amount for combustion. The air is pressurized and heated before it was injected into the combustor to provide the real combustion of microturbines. The heating of the pressurized air was carried out using a low-pressure warm air which was itself heated by an electric heater. Proper ignition equipment is also mounted on the designed combustor which only works during the ignition process.

Control and measurement equipment are also considered to set the desired operating points. The air mass flow rate is adjusted by the electric valve-1 (ECV-1) and ECV-2 and then is measured by the airflow meter with 1% full scale (FS) accuracy. The CO_2 and CH_4 mass flow rates are measured using two mass flow controller (MFC-1 and MFC-2) with an accuracy of ±2% FS. To measure the pressure and temperature, three K-type thermocouples and pressure gauge device is considered in the line. The temperature and pressure of the pressurized air before and after the recuperator and those of exhaust gas from the designed combustor are also measured to keep the operation of experimental rig stable. The emissions (CO_2, CO, NO_X) were measured by a Model 4000VM Heated Vacuum Chemiluminescent Gas Analyzer from a central point downstream of the flue gas pipeline. The measurement accuracy of the (NO_X) and (CO_2) is both 1% FS.

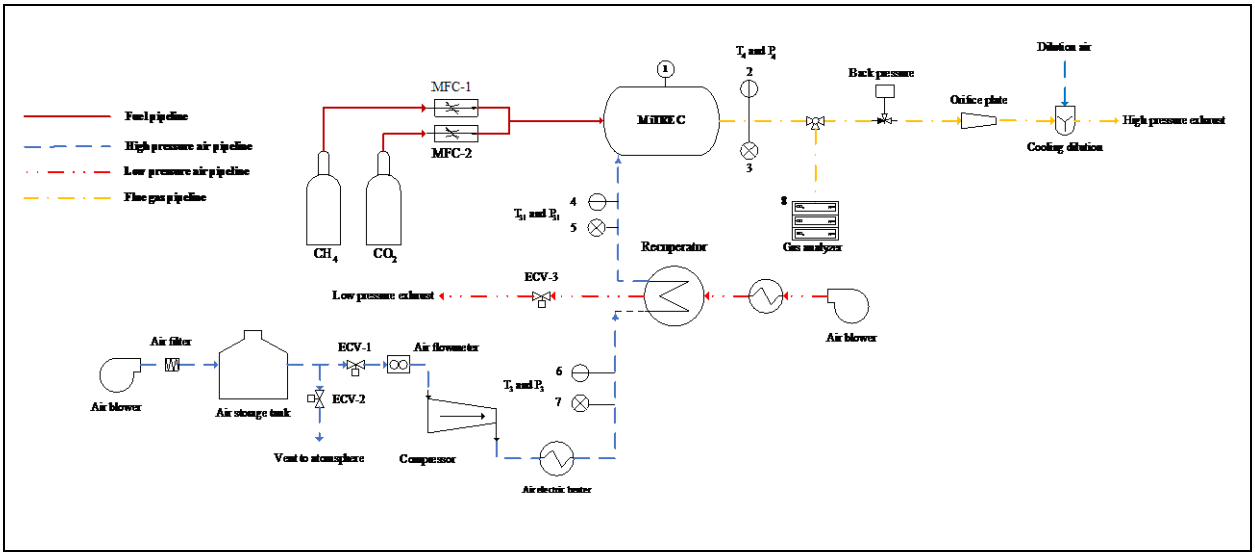

Fig 5 Schematic of experimental setup (1. Ignition equipment, 2. K-type thermocouple, 3. Barometer, 4. K-type thermocouple, 5. Barometer, 6. K-type thermocouple, 5. Barometer, and 8. FTIR gas analyzer)

2.4.3 Ignition, combustion efficiency and pollutants analysis (CO_2,CO, NO_X, and UHC)

The fuel/air ratio should be well below the blow-off limit, so the mixture is lighted. Ignition and extinction of the combustor were tested at the atmospheric condition. For this test, the air and fuel (CH_4+CO_2) injected to the combustor within 5 seceonds were ignited and if they could sustain combustion for 10 seconds, this is a pass lit test. 3 consecutive lights are a successful point. The combustor was lit at 40g/sec airflow with pure methane. With 60% methane, it would not light above 20 g/sec. The combustion efficiency goes up for the combustor outlet temperature above 1050 K. The overall trend of unburned hydrocarbons, CO and combustion inefficiency (1-combustion efficiency) is almost the same. The presence of CO_2 in the biogas impairs both the ignition and combustion. It slightly deteriorates the combustion and decreases combustion efficiency. However, it decreases the NO_X emission.

2.4.4 Validation

The ignition test and durability of the combustor were tested at 35 different operating points for methane and biogas with different concentrations of methane (CH_4) and carbon dioxide (CO_2). The extinction was also observed at some of the defined operating points. Based on the experimental test, NO_X, and CO_2 and temperature at the combustor outlet are used to verify the accuracy of CFD modeling.

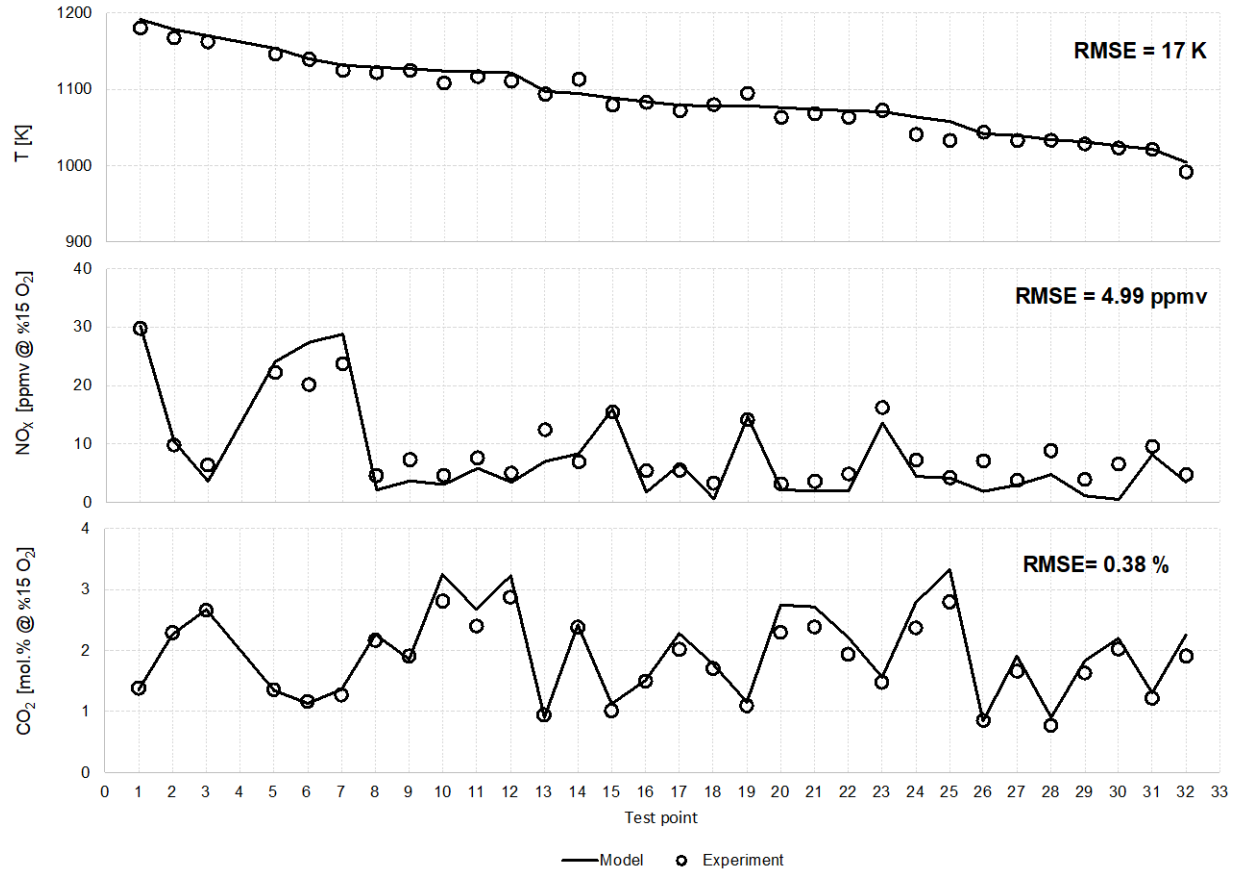

Fig 6 Comparison between the measurements and CFD model prediction at the combustor outlet.

530

531 *2.4.5 Comparison of numerical and experimental test results*

532 The combustor outlet temperature, NO_X, and CO_2 emissions are used to validate the CFD
533 modeling accuracy and comparison between measurement and modeling. The results of the
534 validation test are given in **Fig 6**. The statistical errors of the simulations are presented in Table 2.
535 The coefficient of determination (R^2), average absolute relative deviation (%AARD), root meant
536 square error (RMSE), and standard deviation (STD) are given to show the accuracy of the
537 modeling and variability of experimental data tested.

For all measurements, the experimental values are very close to numerical simulations. The deviation among the modeling and experimental results are mainly due to the oscillations that occurred during the tests to keep the operating points to their desired values. This comparison shows that the CFD method is well able to analyze the performance of the combustor in terms of both micro and macromixing.

Table 2 The statistical errors of the combustion mechanisms

No	Variable	Statistical errors			
		R^2	%AARD	RMSE	STD
1	Temperature	0.99	0.43	6.17	210.63
2	CO_2	0.95	6.48	0.11	1.27
3	NO_X	0.85	21.25	3.72	44.96

3. Result and discussion

After the chosen CFD model was verified and validated, it was used for the further analysis of the combustor. The results from the simulation are used here to analyze the operability of the Bladon microturbine at the company Iso conditions. The combustor characteristics including recirculation zone, overall pressure loss, temperature distribution, and flue gas composition are targeted for the analysis of combustor characteristics using CFD. The operation of the combustor in the energy efficiency of the microturbine is also investigated to see the operability of biofuels in powering the turbines. Afterward, the final advantages and benefits of the combustor using renewable fuels are mentioned and summarized.

3.1 Combustor characteristics

In this part, the combustor characteristics including combustor efficiency, pressure loss factor, temperature distribution, and flue gas composition are analyzed. The CFD tools including the

models and numerical schemes are also used for simulation of other fuels in the combustor and make comparisons among various fuels.

3.1.1 Flow pattern (recirculation zone and features of the velocity fields)

For combustion to sustain in the designed combustor, recirculation of hot partially reacted products is needed to ignite the fresh flow of fuel and air. Appropriate establishment of the recirculation zone in the combustor also leads to flame stabilization by providing partially reacted material for the combustion and controlling the boundaries of the flame in the liner. The velocity field of the combustor is a useful case to show the flow patterns in the combustor. The flow characteristics of the flow fields in the burning case are demonstrated in **Fig 7** by the streamlines of two longitudinal planes (YZ, YX) for biogas fuel and bioethanol. It shows the appearance of three recirculation zones: primary recirculation zone (PRZ) and secondary recirculation zone (SRZ) and cooling recirculation zone which have been also confirmed through Loughborough experimentation. The PRZ forms in the central jet vortex around liner shoulder because of the shoulder structure, swirling intensity, swirling angle. The establishment of PRZ is partly due to the appearance of the centrifugal force in swirling air as a result of the change of its radial to axial velocity. The CRZ is formed because of the low flow velocity near the liner head and vortex appeared by injection of through head cooling holes which is less intense that PRZ. The main objective of CRZ is to chill the combustor head and keep the temperature in solid walls well below the steel melting points. The SRZ appeared in the center of the combustor in the fuel jet stream. The SRZ leads to better mixing of the fuel and air, sustainable combustion, and high combustion intensity in the combustor primary zone. The appearance of both PRZ and SRZ is mainly resulted from the interactions among the central core swirling vortex with high impinging primary jets, which drive the backflow in the primary region. The impingement of the primary jets here alters

the flow configuration in the combustor primary zone. In the case of liquid fuels, the intensity of SRZ is a bit inferior compared to gaseous fuel in the primary zone of the combustor. This is mainly due to the interactions among the liquid droplets and highly reacting turbulent flows. Indeed, the high velocity liquid droplets which is being sprayed with 45^{o} and are denser in the middle could invigorate the fluid within the chamber, resulting in lowest intensity of SRZ. In this case, the PRZ does still exist leading to sustainable liquid combustion. The CRZ is also still available leading to effective combustor head cooling. The importance of backflow in flame stabilization has been also confirmed by Di mare et al. [69] using large eddy simulation (LES) turbulence modelling for a similar combustor with their results compared with experimentation.

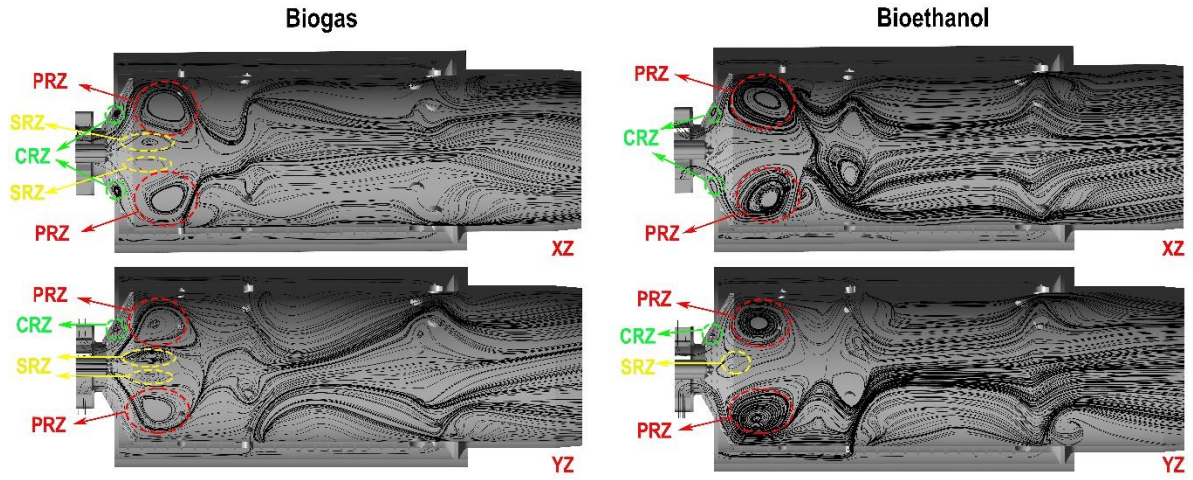

Fig 7 Streamline distributions at two longitudinal cross planes (YZ, and XZ)

The flow characteristics downstream of the fuel nozzle is less under the influence of the fuel injector and swirler conditions. **Fig 7** showed that the injected air from the swirler to the chamber can successfully surround the fuel jet, hampering the encroachment of the flame to the liner inner walls. This near-wall movement of the swirl air was then partly pushed back in the vicinity of the primary ports via interactions by primary air. In **Fig 8**, the impingement region of the combustor primary is shown for two biogas and bioethanol fuel. It is evident that centripetal primary air jet

599 can successfully penetrate the coaxial movement of the fuel and air mixture by forming an oval
600 vortex around the combustor axis. This could not only lead to the flame stabilization in the primary
601 ports but also a better mixing and completion of the combustion further downstream. The
602 penetration depth of primary air is high enough to surround the biogas jet limiting it from
603 expanding downstream. In the case of bioethanol, the impingement region has apparently more
604 depth which could be likely to uniform spraying of fuel in the chamber and complete vaporization
605 of it before the primary holes. The secondary jet intensity, as it is shown in **Fig 8**, is high enough
606 to behave similarly as the primary jets, by surrounding and finally mixing with the mixture. The
607 secondary holes are considered for this case as the dimensions of the micro combustor are
608 relatively small and the strategy of air staging is essential for control of NO_X emission. Further
609 downstream, there are two series of dilution holes embedded in the body of the liner for the final
610 cooling of the mixture and reduction of NO_X significantly. The structure of the flow at dilution
611 ports, as shown in **Fig 8**, is of a different nature. The crossflow pattern at the dilutions holes is
612 rather asymmetric. This is likely associated with the passage of the air immediately downstream
613 of the dilution ports from a circular liner to the conic discharge nozzle. **Fig 8** approves that the jet
614 penetrations at both series of dilution holes (1 and 2), especially series 1, is proper for complete
615 mixing with the mixture and reduction of NO_X.

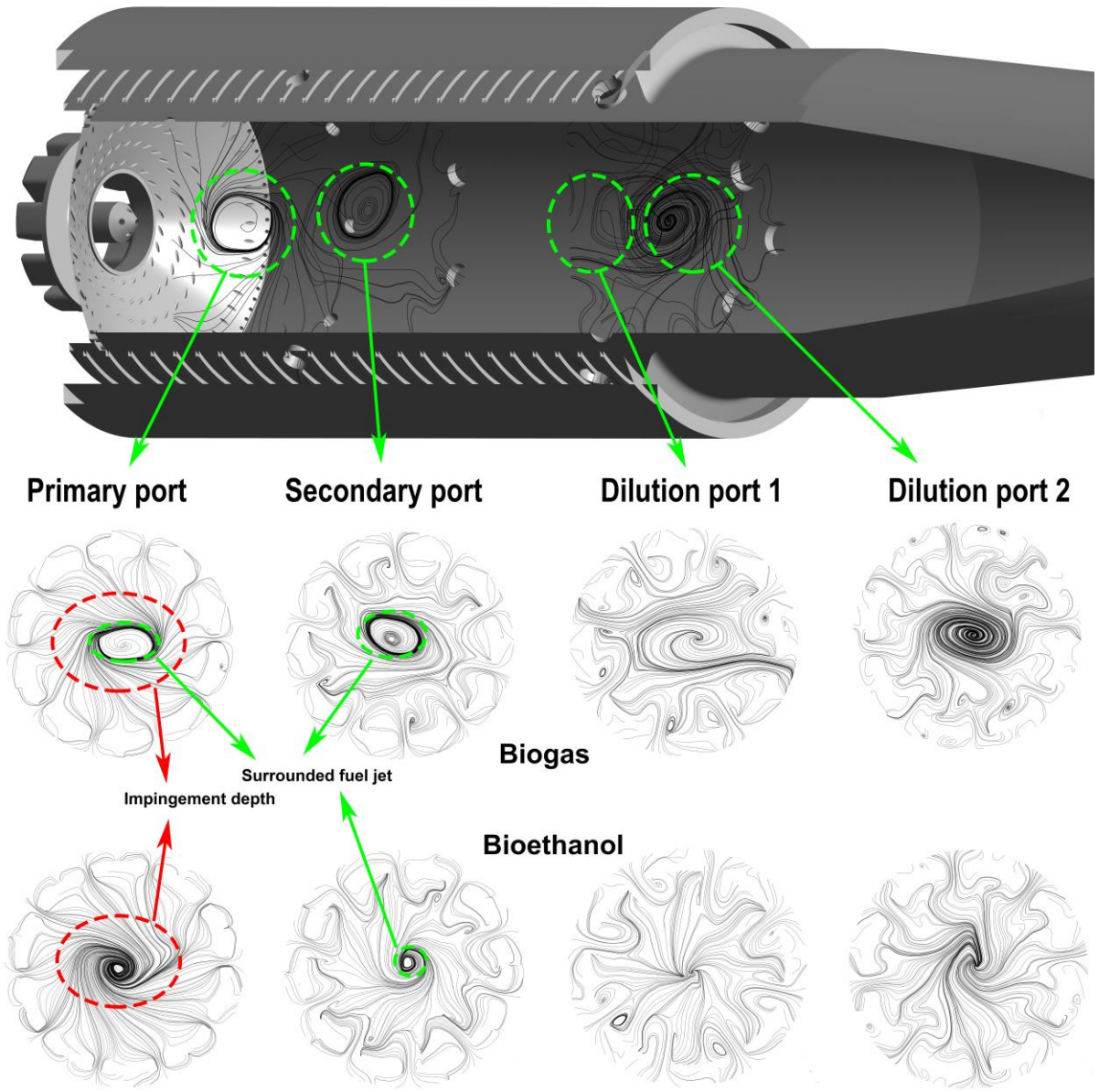

Fig 8 The combustor radial streamlines at the cross sections of the combustor at primary, and two series of dilution port.

616

617 *3.1.2 Overall pressure loss*

618 The σ is given in **Fig 9** along the combustor axis. The combustor axis is defined as a line in the

619 middle of the combustor starting from the nozzle inlet plant ending at the combustor outlet plane.

Fig 9 bigger subplot demonstrates σ along the axis covering the pressure loss factor in only the combustor excluding the fuel nozzle. For better clarification, in the smaller subplot, the σ over the entire length of the axis is given. The designed combustor can satisfy the overall allowable pressure drop giving rise to the facility of fluid movement therein and appropriate aerodynamic of the combustor components. The combustor pressure drop in flame holder could be mainly influenced by the combustor opening (primary, secondary, and dilution ports), swirler and fluid pressure drop due to the sudden compression, expansion, frictions. The combustor pressure drop is well below 1% of the desired 297 kPa which is low enough for the turbine to work normally. This figure also confirms that the final compression of the fluid in the discharge nozzle could not drop the pressure less than the desired limit.

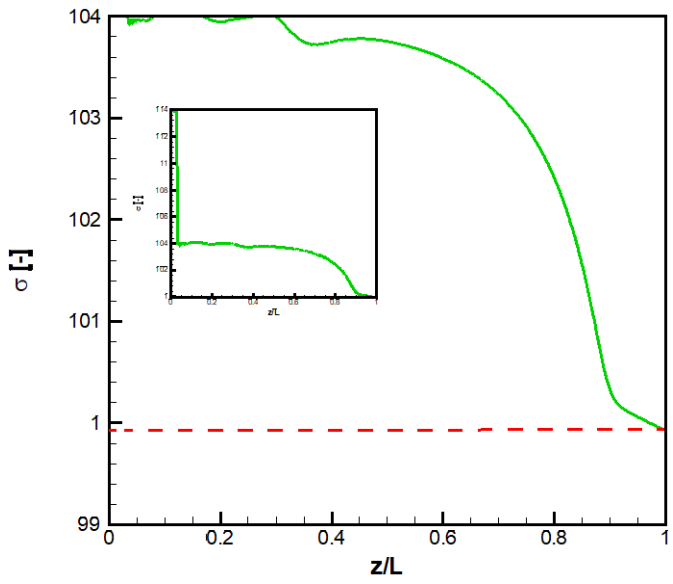

Fig 9 pressure loss factor (σ) along the axis of the combustor.

3.1.3 Combustor temperature and Outlet temperature distribution

The temperature profile is analyzed here. The contour of the temperature on the combustor solid walls is given in **Fig 10**. The combustor solid temperature is obtained by modelling the convective

heat transfer from the reactive material within the combustor to the solid parts, and conductive heat transfer through the solid parts and finally natural convective heat transfer from the solid parts to the environment (recuperated air). The temperatures at both inner and outer walls are given in Fig 10. which are well below the stainless-steel melting points. The maximum temperature of the solid walls (1049.85 ^{o}C) is observed in the combustor inner walls near the secondary ports where the air for the complete combustion of the fuel is provided. Another part that is prone to comparatively high temperatures is the area of the combustor after the dilution holes. This is likely due to the fact that fluid in this area of the combustor is on the threshold of compression as it enters the discharge nozzle. The decrease in the area for the passage of the fluid forces some part of it towards the walls, as a result, increasing the temperature appreciably. However, the temperature of the discharge nozzle walls decreases further downstream as the dilution air mix with the mixture and decrease its temperature.

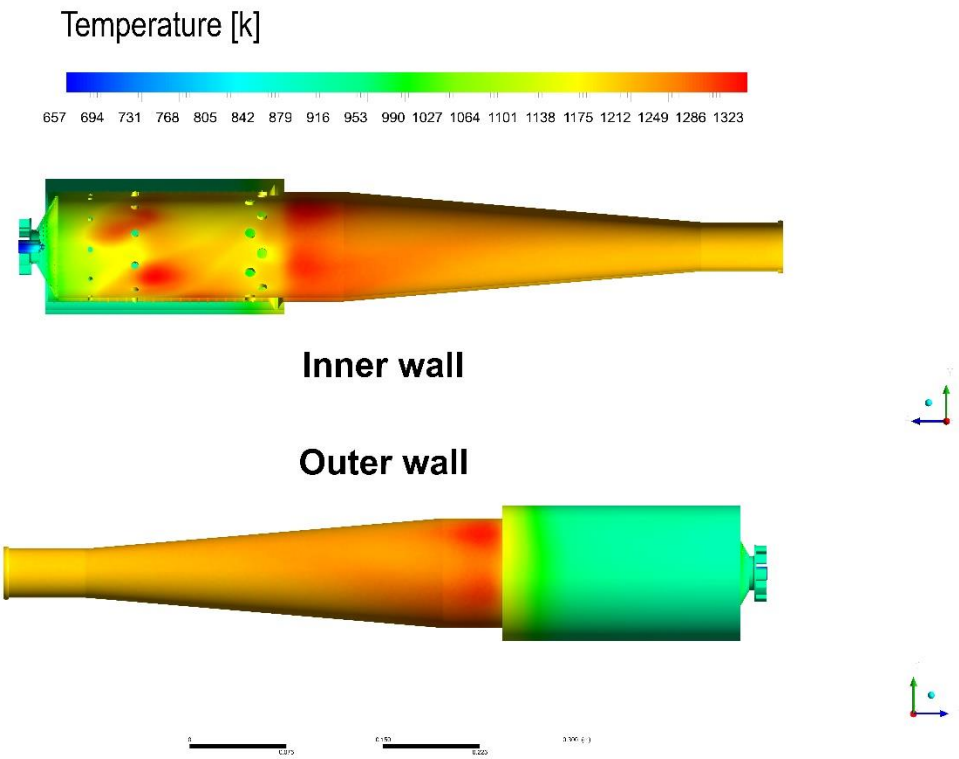

Fig 10 The combustor inner and outer wall solid temperature.

The outlet wall temperature and outlet temperature distribution factor are given in **Fig 11** along the radius of the combustor outlet exit plane. The combustor outlet exit plane is in the YX plane. The temperature characteristics of the outlet are demonstrated along the X (Y=0, Z=L, combustor length) and Y (X=0, Z=L, combustor length) coordinates. Uniform radial temperature distributions at the combustor outlet are obtained with a slight variation which is in the range of desired Bladon Iso requirements and far from being detrimental to the MT compressor (two subplots of **Fig 11**). The outlet temperature distribution factor is also given in the downer subplots of **Fig 11**. The circles signify radial distances that OTDF rises significantly, as a result, the local outlet combustor temperature is almost the combustor average temperature. In other radial distances, OTDF

654 $(T_{e,\max} - T_{e,ave})/(T_{e,ave} - T_k)$ is low and almost zero. This is owing to the nominator of the OTDF

655 ratio which is significantly lower than the denominator. The nominator $T_{e,\max} - T_{e,ave}$ represents the

656 difference between the maximum and average temperatures while the denominator gives the

657 difference between the temperature and average temperatures. This trend shows that the average

658 and maximum temperature is almost the same at the combustor exit plane which is the prerequisite

659 for a successful combustor design.

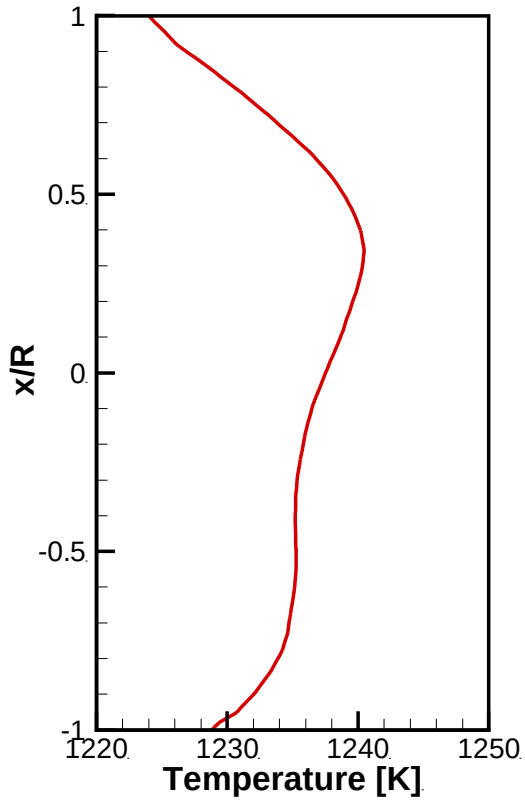
1
0.5
0
-0.5
-1
x/R
1220
1230
1240
1250
Temperature [K]

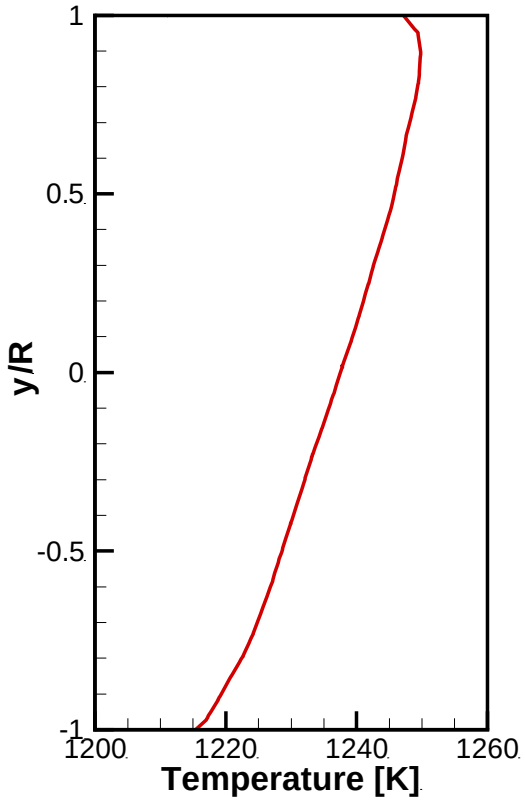
1
0.5
0
-0.5
-1
y/R
1200
1220
1240
1260
Temperature [K]

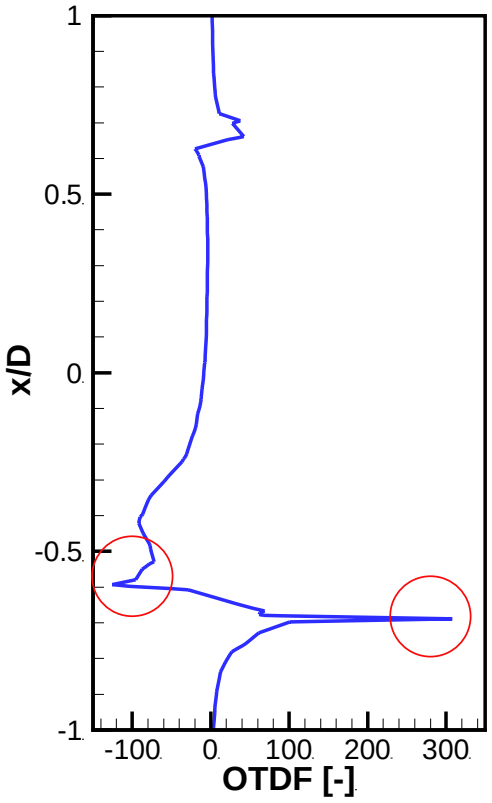
1
0.5
0
-0.5
-1
x/D
-100
0
100
200
300
OTDF [-]

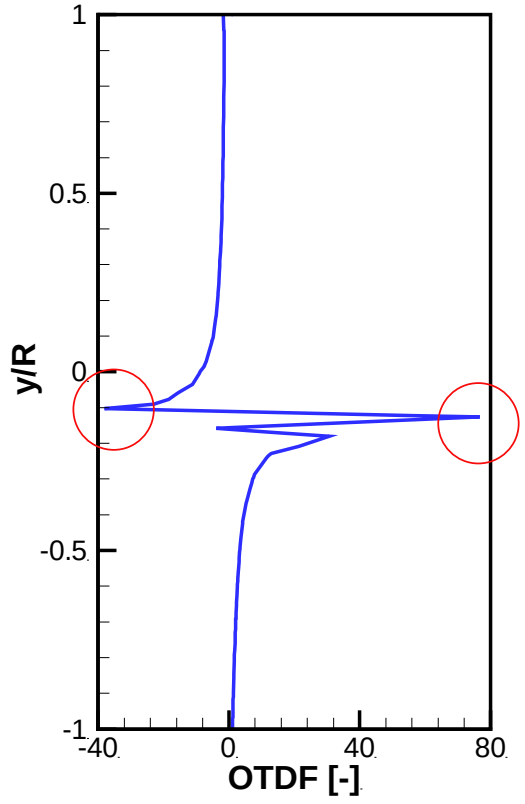
1
0.5
0
-0.5
-1
y/R
-40
0
40
80
OTDF [-]

Fig 11 Outlet temperature and outlet temperature distribution factor at the combustor exit plane.

3.1.4 Combustion efficiency

The combustion efficiency and flue gas composition for the design of the combustor is analyzed in this part using the CFD tool. The ability of the designed combustor to accommodate different renewable fuels prevalent in the market including dimethyl ether, biodiesel, bioethanol, and biogas is verified so as to determine the verity of naming it as MiTREC (microturbine renewable energy combustor). The combustion of diesel and natural gas fuel is also examined compared with the investigated renewable fuel so as to show the flexibility of the microturbine combustor as well as its prospective advantages by using renewable fuel as the primary energy source.

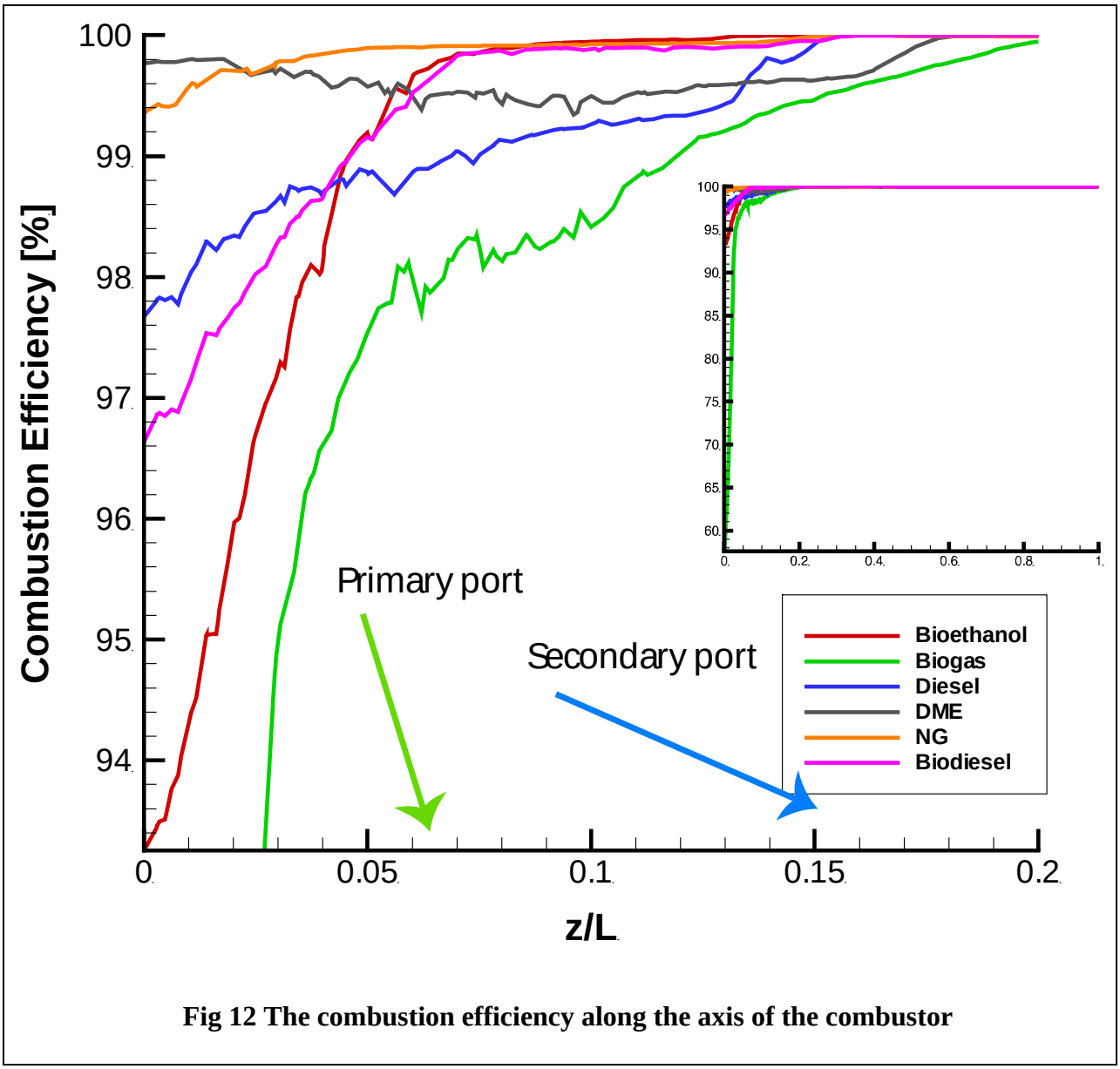

Fig 12 The combustion efficiency along the axis of the combustor

668

669 **Fig 12** depicts the trend of combustion efficiency (h) for different biofuels in relation to z/L(z:
670 direction along the axis from the nozzle inlet to the combustor outlet plane L: total length of the
671 combustor). This figure shows the evolution of combustion efficiency for different fuels. It is
672 evident that the combustor can well accommodate the range of hydrocarbon and renewable fuels.
673 The combustion efficiency for all fuels reaches almost 100% just before the dilution holes in the
674 vicinity of secondary ports. The increasing rate in combustor efficiency of biogas is rather slower

than other fuels which is likely due to 43% carbon dioxide in the fuel jet. CO_2 is an impurity in biogas fuel. It leads to poor mixing of biogas methane with air as well as decreasing the combustion temperature. This results in slower increasing trend of biogas combustion efficiency along the combustor axis. Biogas combustion efficiency reaches almost 100% at z/L=0.2 well before the dilution holes (dilution holes $z/L \cong 0.3$). This means that the designed combustor is capable of completing the combustion of whatever the fuel. The amount of air injected through swirler, head cooling, primary and secondary ports, the rate of mixing of fuel and air is high enough for high quality complete combustion. The h for liquid fuels (bioethanol, biodiesel, and diesel) evolves slower comparatively than for other gaseous fuel. In general, **Fig 12** authenticates that the designed combustor completes the combustion for whatever the fuel before the dilution ports ($z/L \cong 0.3$).

3.1.5 Flue gas composition

The analysis of the flue gas in the combustor is given on the combustor axis and outlet in terms of the CO and NO_X concentrations and CO_2 mole fraction. For this combustor, the level of the gaseous emissions was corrected based on 15% excess dry air in mixture excluding water [70]. A comparison also made between the range of renewable fuels investigated. **Fig 13** gives the axial level of CO_2 [mol.%], CO [ppm**]**, and NO_X [ppm] emissions in relation to the combustor middle line.

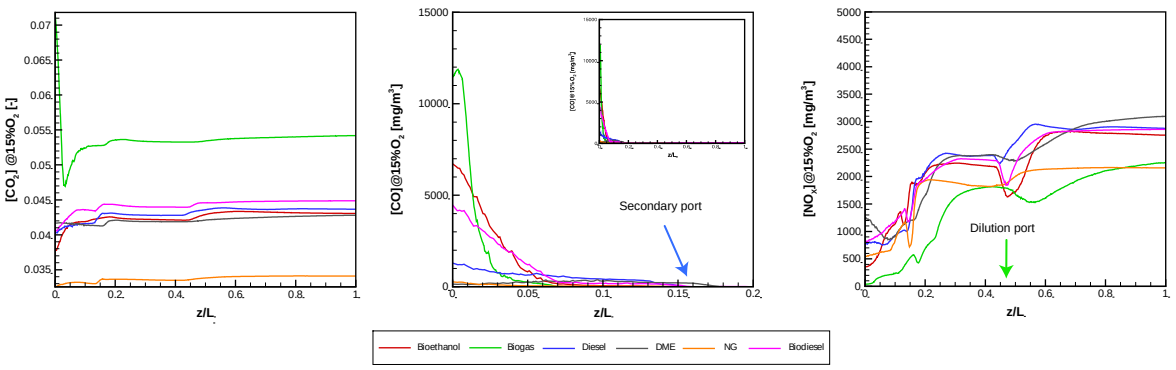

Fig 13 level of gaseous emission (CO_2 [mol.%], CO [ppm], and NO_X [ppm]) along the combustor axis based on 15% excess air.

692 The CO_2 emission in mol% is compared and given for the fuels on the combustor axis. When the
693 combustion is complete, CO_2 emission is controlled by the carbon content in different fuels [71].
694 Thus, the comparison between the CO_2 of fuels is valid after the dilution holes. As expected, the
695 highest level of CO_2 emission corresponds to biogas, while the lowest is for NG. For other fuels,
696 the comparative highest to the lowest level of CO_2 is in respective for biodiesel, diesel, bioethanol,
697 and DME. Note that CO_2 for biofuels is completely renewable imposing no extra charge and
698 damage during the operation of the microturbine.

699 Carbon monoxide (CO) is an intermediate product of the combustion-hydrocarbon-oxygen
700 reaction which is controlled by partial mixing as well as local low combustion temperatures [72].
701 The axial trend of CO emission showing that the combustion completes after the secondary holes
702 for almost all fuels. Thus, the level of mixing, spatial temperatures, and position of openings in the
703 design are well-chosen leading to high-quality combustion and lowest possible CO emission at the
704 outlet. When the combustion air is enough, and combustor could provide an appropriate level of
705 mixing, CO formation is probable on the cold combustor parts, as a result of the flame extinction

and quench of combustion reactions on the cold surfaces. Compared to other fuels, the highest CO is obtained at the combustor axis for biogas fuel. This is likely due to the existence of associated carbon dioxide in the methane which makes the initial mixing ineffective and combustion incomplete more likely.

In this analysis, NO_X is a mixture of NO, NO_2 and N_2O. The evolution of NO_X at the combustor axis is also analyzed here. This analysis shows that the NO is the main component of NO_X. The NO forms in the combustor through thermal and prompt mechanisms [73]. These mechanisms depend highly on the combustor local temperatures [74]. The axial NO_X trend shows that it is under control in the designed combustor. Indeed, the design strategy of air staging through primary and secondary ports hampers the NO_X in the combustor to rises significantly. The dilution holes could effectively control the NO_X and suppress it from rising significantly. It also controls the combustor outlet temperature and set the desired MT inlet temperature. While, there is a high tendency for NO_X to elevate in the combustor, effective air staging strategy (air distribution) and proper embedded locations of holes in the body of the keep the spatial NO_X emission under the control.

The area-averaged level of gaseous emission is given at the combustor outlet for the fuels. The level of CO_2 emission in molar percent, CO and nitrogen oxides in molar fraction (ppm) of the dried flue gas with 15% oxygen content are given in **Fig 14**. The lowest to the highest level of CO_2 emissions is for Natural gas, DME, diesel, bioethanol, biodiesel, and biogas, respectively. Except biodiesel, the level of CO emissions for biofuels (bioethanol, DME, and biogas) is nearly zero, giving rise to the efficient combustor operation with a range of fuels. The level of nitrogen oxides- NO, NO_2 and N_2O at the combustor outlet shows that DME, natural gas, biodiesel, diesel, bioethanol, and biogas has respectively the highest to the lowest NO_X.

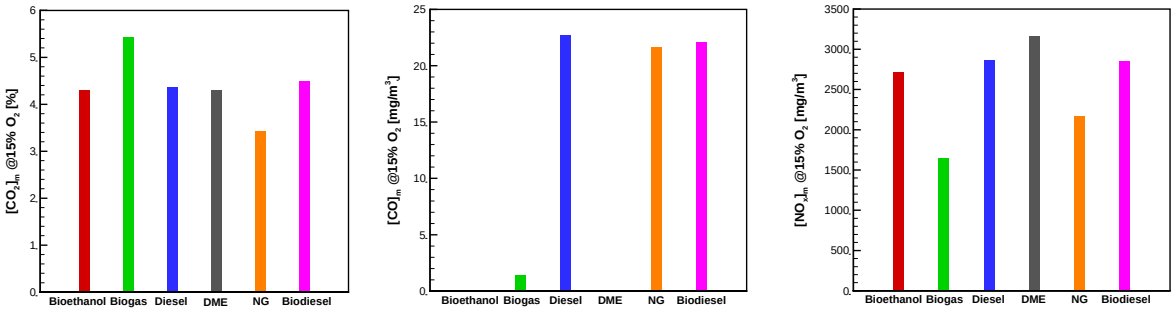

Fig 14 average level of gaseous emissions at the combustor outlet plane.

3.1.6 Flue gas composition

The operation of the current design is compared with other MT turbine combustors. The results are given in Table 3.

Table 3 Comparison between the MiTREC and other MT combustors

Combustor	Characteristics				
	Fuel	*s*	*h*	NO_X	Reference
MiTREC (12 kW)	Biofuels	<1%	>99%	[10 100]	Current work
MTT (5 kW)	GAS	<1.5%	>99%	[20 140]	[75]
KTURBO (20 kW)	Oil	≅ 4%	≅ 99.5%	[5 60]	[76]
Elliott TA80R (80 kW)	NG	≅ 5%	>99%	48	[77]

3.2 Energy optimization

The main goal of optimization aimed for the combustor in the MT cycle is to determine the fuel and air mass flow rate at various MT conditions including temperature, pressure, and inlet fuel composition. The device for optimization the Gibbs free energy minimization, $\left(dG^t\right)_{T,P} = 0$ [78]. In this approach, the operation of the combustor in MT will be adjusted so as the thermochemical state of the system is thermodynamically favorable and stable. At this condition, the total Gibbs

free energy is minimum with its gradient zero under the desired optimum conditions (temperature, pressure, and fuel mass flow rate) [79]:

$$G^t = \sum n_i \Delta G_{fi}^0 = \sum n_i RT \ln\left(\frac{f_i}{f_i^0}\right) \quad (8)$$

In this equation, n_i indicates the number of moles; G_{fi}^0 is the standards Gibbs energy of the formation; R is the universal gas constant; T is the temperature; f_i is the fugacity of pure element i; f_i^0 is the fugacity of pure elements at the standard state.

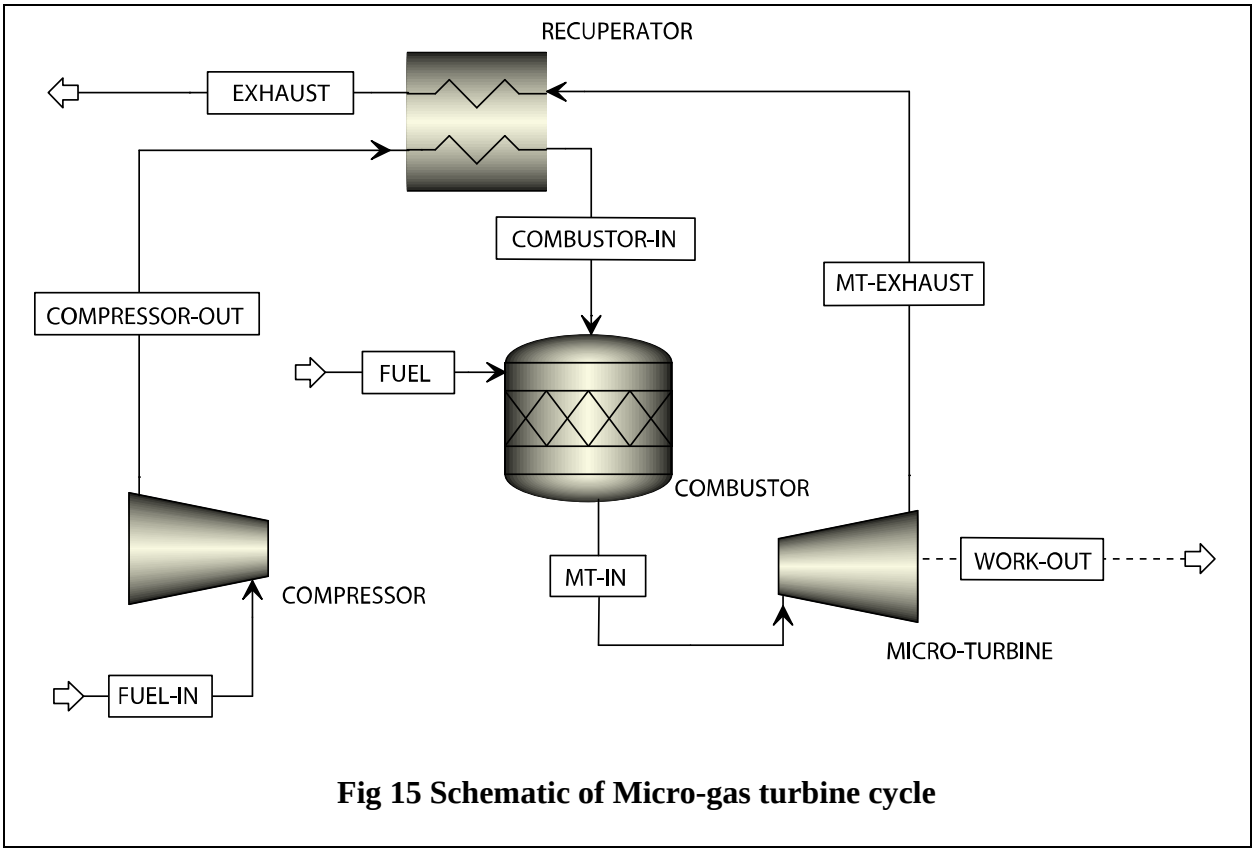

Fig 15 Schematic of Micro-gas turbine cycle

The newly designed combustor is to be used in the MT cycle to drive 12 kWe power shaft. The schematic of the Bladon MT streams could be simply drawn in the standard MT cycle as in Fig 15. The first law of thermodynamic governs that the enthalpy of exhausted gas from the MT is transferred to the compressed air. The energy efficiency of using thermochemical heat recovery depends on the enthalpy of the exhaust gases entering the recuperator and compression ratio of the

combustion air. For this MT cycle, the combustor and the fuel have been changed which could only impact the energy exchange within the combustor and recuperator. The application of combustor in recuperator could improve the efficiency of the Bladon MT cycle as it did so in other similar circumstances [80]. Hence, an objective function including both the recuperation and combustor duties is defined as follows:

$$OF = Q_{COM} + Q_{REC} \quad (9)$$

where Q_{COM} and Q_{REC} denote the energy created and exchanged within the combustor and recuperator per 1 kg of intake. This definition was enough for the optimization purpose of the turbine overall as a new choice of fuel and combustor mainly influence this part of the MT cycle. The combustor was designed for an available microturbine plenum without any required changed in other parts (compressor, turbine, etc).

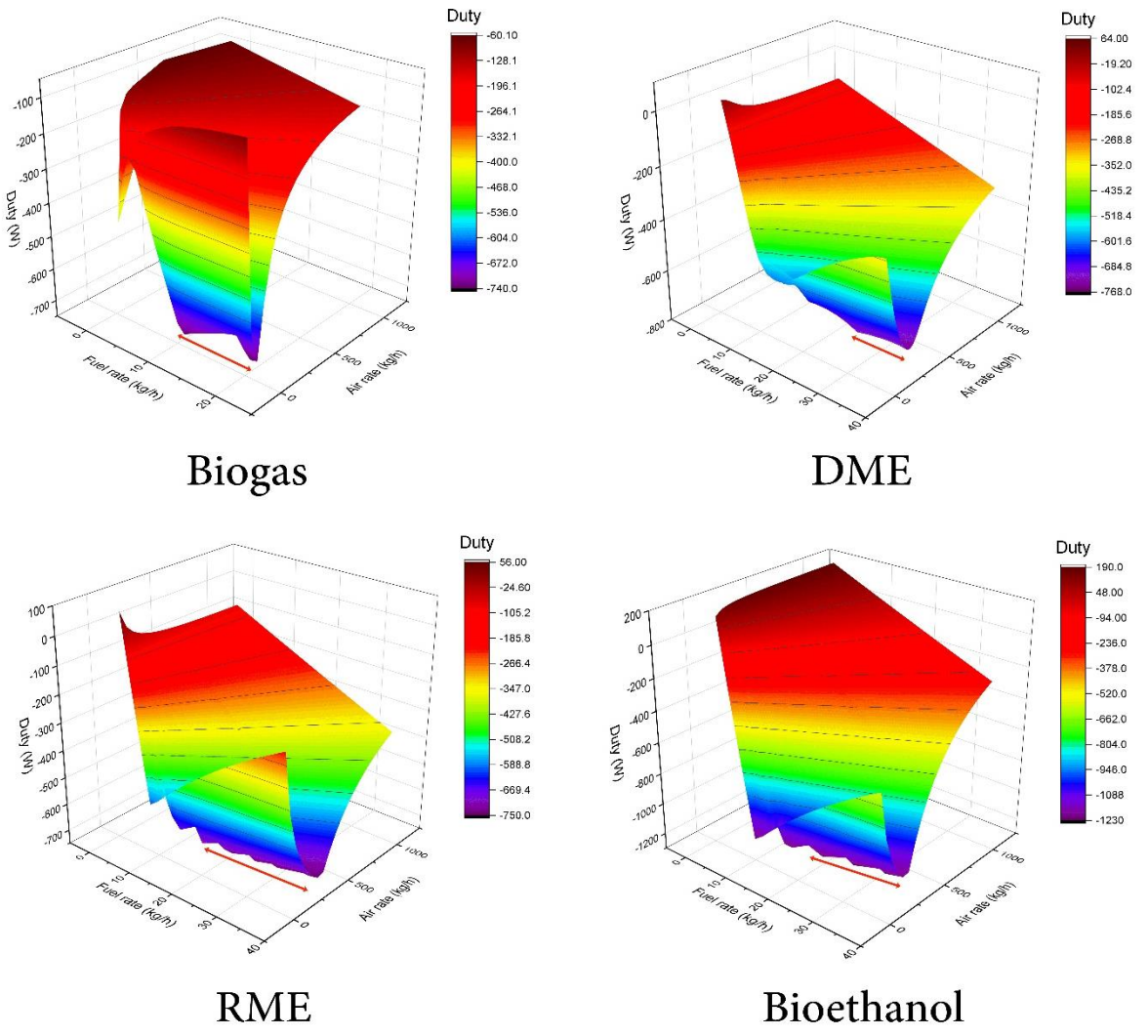

Fig 16 The objective function optimization at fuel and air flow rate for biogas, DME, RME, and biodiesel

Optimization aims to minimize the objective function, meaning that at the constant energy output from the turbine, maximum combustion energy, or the energy released in the combustor, will be reused in the recuperator. **Fig 16** demonstrates the results of optimization for independent variables: fuel and air mass flow rates. The heat regeneration from the turbine exhaust will be maximum at the minimum part of curvature which is in purple. The area of optimized mass and airflow rates is also marked in **Fig 16** via two barbs. **Table 4** gives the specific fuel and air mass

flow rates at the optimized conditions for renewable fuels. Dmitry Pashchenkov [79] revealed that operational parameter including pressure, composition of inlet streams and temperatures play a key role on the energy system of exhaust heat recuperated systems.

Table 4 Optimized operating points for the operation of MT

No	Fuel	Optimized variables		
		$\dot{m}_{fuel}[kg/h]$	$\dot{m}_{air}[kg/h]$	OF
1	Biogas	19	106	-738
2	DME	32	284	-766
3	RME	34	390	-750
4	Bioethanol	32	284	-1226

3.3 Fuel energy and recuperation analysis

The operability of the newly designed combustor was evaluated and compared with the conventional use of diesel and natural gas in a recuperated micro-gas turbine cycle for the optimum conditions. The energy efficiency including cycle and recuperator efficiency and exergy analysis of the new combustor is evaluated. The operation of the micro-gas turbine with recuperated air system ideally follows an open Bryton cycle plus an air regenerator (i.e., recuperator). For fuel energy and recuperation analysis, the new combustor with renewable fuels is tested under ideal microturbine condition for 12 kWe net output water. For this analysis, the air is taken from the atmosphere (Coventry weather conditions; Pressure 1 bar; T= 298 K) and compressed to 3 bars, then it will oxidize the biofuels. Finally, the hot gases go through the turbine and exit the recuperatur shell at 1.6 bar and T=552 K. Different fuel could perform differently in the MT cycle according to different quantities needed and different composition of the flue gas. The T-S diagram of simulation for renewable fuels and natural gas superimposed by that for diesel fuel is given in

Fig 17. In the case of biogas, it is specifically compared to natural gas firing MT counterpart. The effectiveness of the recuperator ($e = \frac{q_{recup,act}}{q_{recup,\max}}$), the thermal efficiency of the cycle $h_{thermal} = 1 - \frac{T_{MT-IN}}{T_{AIR-IN}}\left(r_p\right)^{\frac{k-1}{k}}$ [81] in the microturbine are shown in **Fig 18**.

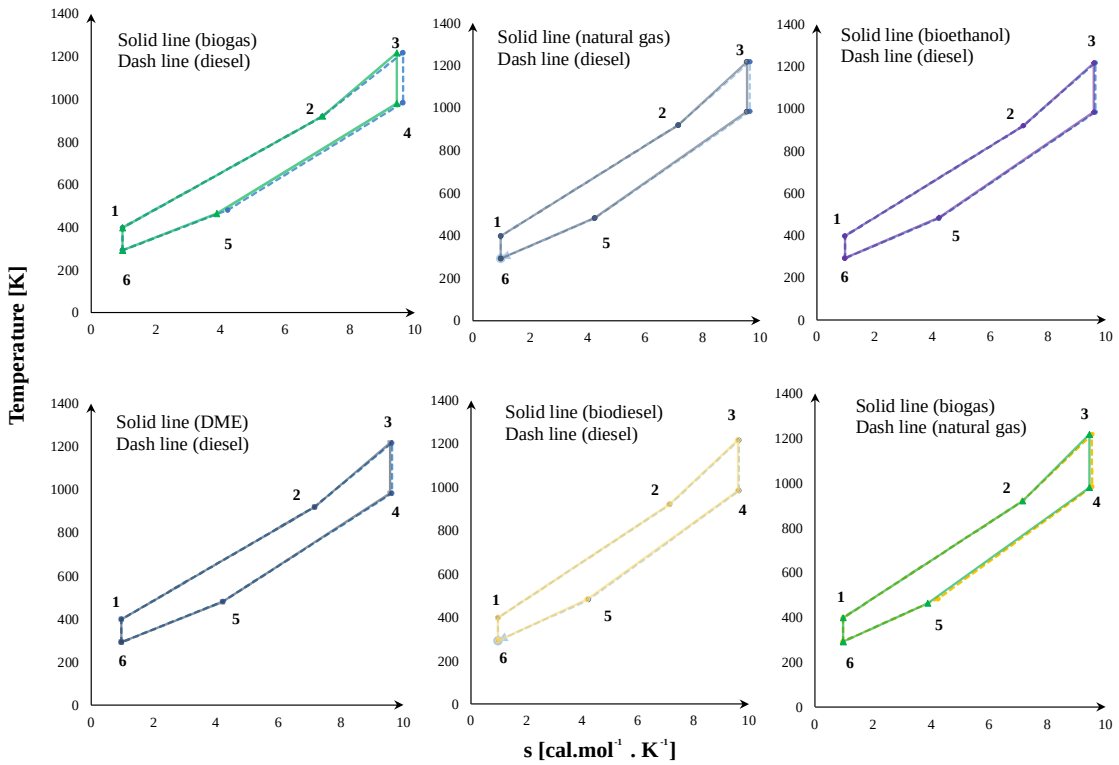

1. Air-In, 2-Compressor-out, 3. Combustor-in, 4. Combustor-out, 5. MT-Exhaust, and 6. Exhaust

Fig 17 T-S diagram of the 12 kWe output microturbine cycle with renewable fuels

The recuperator effectiveness for renewable fuels is compared in **Fig 18**. It is around 0.897 for biogas fuel and 0.89 for other renewable fuels. The cycle efficiency figure is generally similar to the MT efficiency with biogas possesses the maximum efficiency. The MT efficiency with one pass recuperator with biogas fuel is around 16% and for other renewable fuel could be around 15.6%. De Campos et al. [82] have revealed that an optimized closed cycle 100 kWe micro turbine

804 efficiency is around %30 and that appropriate choice of working fluid could increase the efficiency
805 to a upper limit %35.

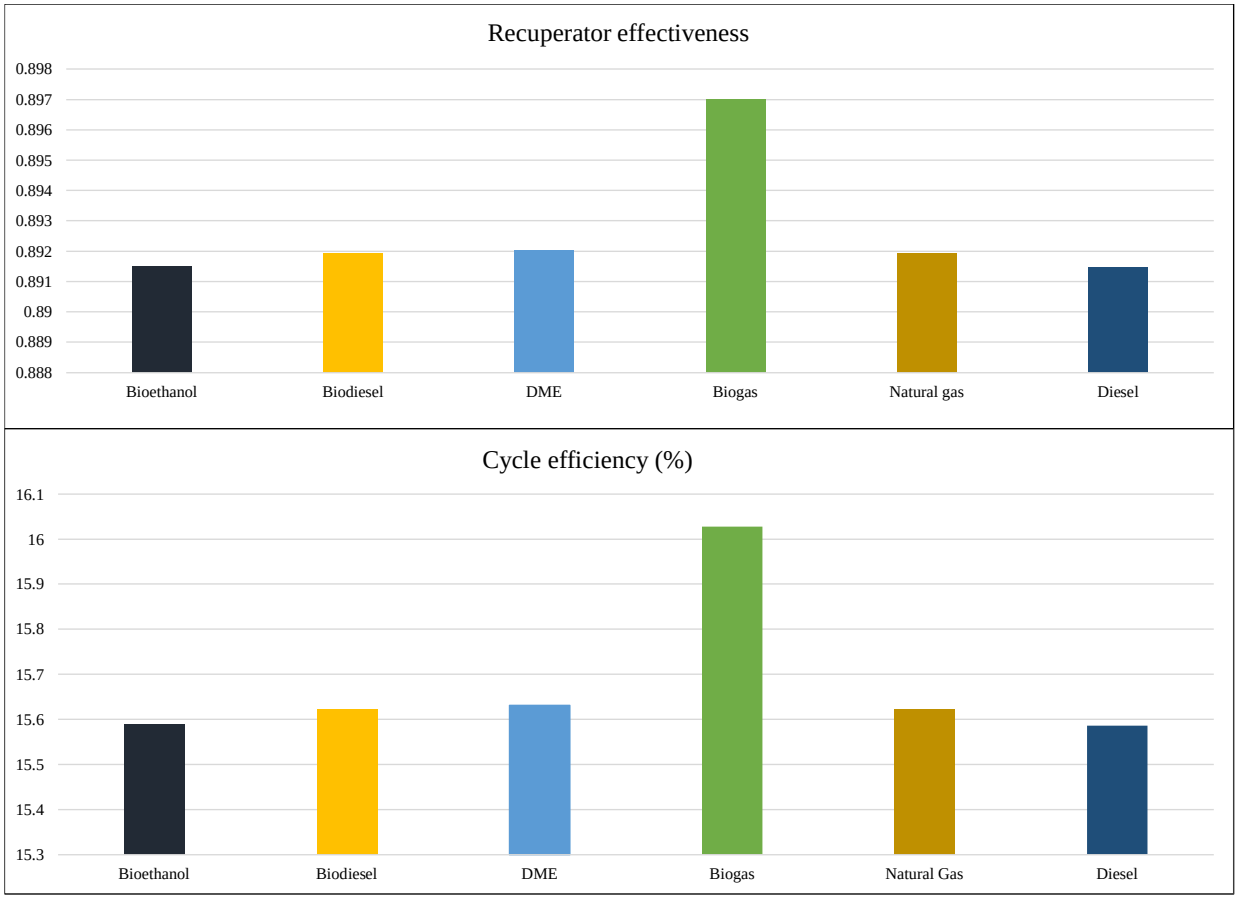

Fig 18 Recuperator effectiveness and MT cycle overall efficiency with the new designed combustor

806 *3.4 Irreversibility with new combustor*

807 The inefficiency of the MT in the use of available renewable energy due to irreversibility can be
808 represented by exergy loss. In contrast to the energy, the exergy of a closed system is not conserved
809 [83].

810 $$\sum_{\text{into the cycle}}\left(\dot{n}\ \text{ex}+\dot{\text{Q}}\left(1-T_0/T_s\right)+\dot{W}_s\right)-\sum_{\text{out of cycle}}\left(\dot{n}\ \text{ex}+\dot{\text{Q}}\left(1-T_0/T_s\right)+\dot{W}_s\right)=\left(Exergy\right)_{destroyed} \quad 10$$

811 The total rate of exergy loss represents the overall thermodynamic imperfections, which is
812 directly proportional to the rate of entropy production due to irreversibility in a column operation.
813 In this case, the exergy loss of MT with the designed combustor fueled with different fuels is
814 reported **Fig 19.**

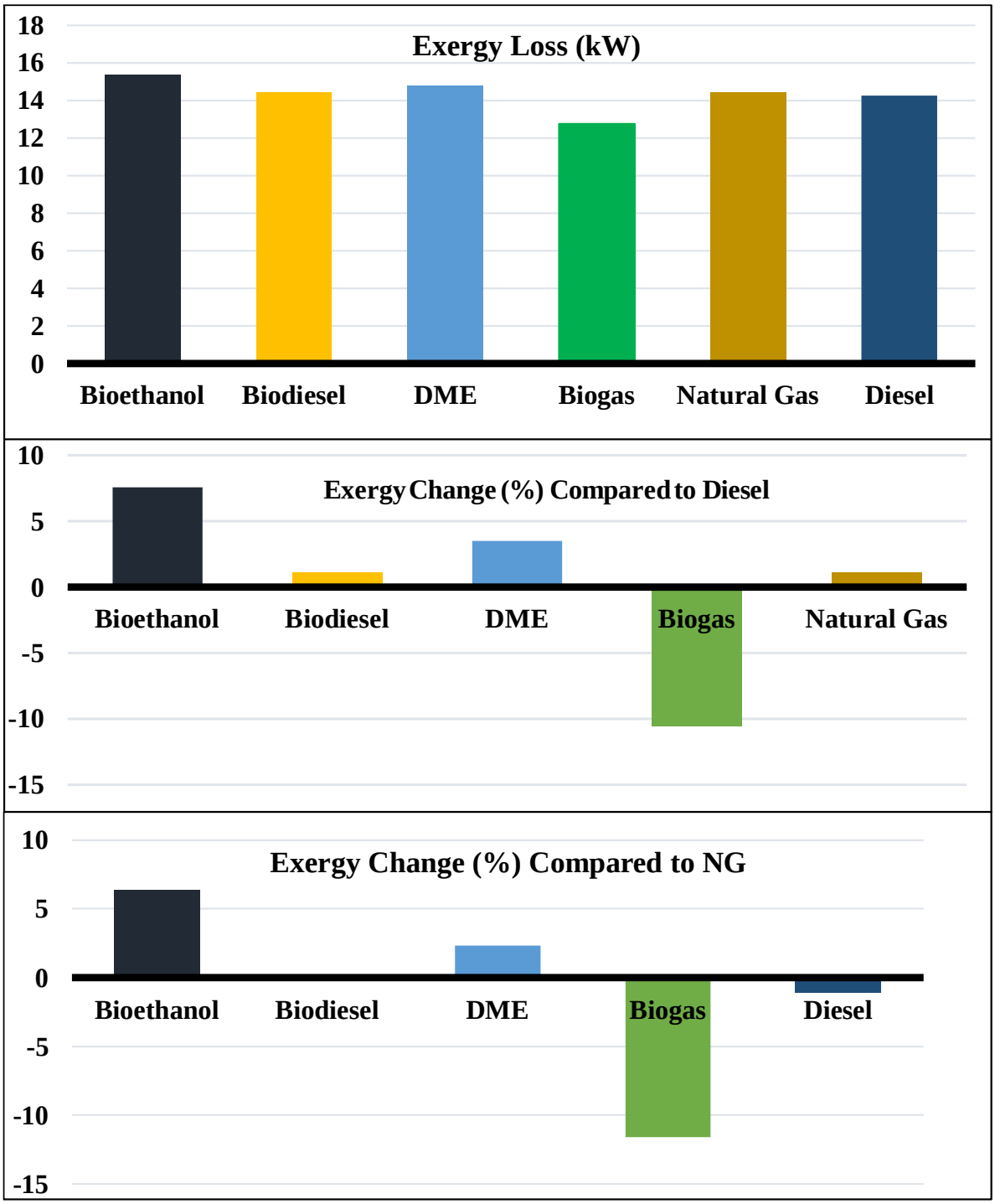

Fig 19 The absolute exergy loss of the MT cycle with new combustor fueled with biofuels and percentage of change when considering replacement with diesel and natural gas fuel

Microturbine parts mainly responsible for exergy destruction and losses are combustion chamber and recuperator. The exergy losses from these two components are mutually related which could be minimized with a good system optimization approach. Another part of exergy loss is intrinsic which could not be easily eliminated and due to the flow frictions, manufacturing and design constrains. Here, the exergy loss from the fluid flow is analyzed [84]. Compared to diesel and NG, the biogas fuel leads to 11% and 12% reduction in exergy loss of the MT cycle, respectively. For other fuels, an increase in exergy loss from MT is observed. Using bioethanol, and DME as a replacement for NG, the exergy loss increases by 6% and 2%, respectively. The biodiesel, however, has the same exergy loss of NG in MT. The bioethanol, biodiesel, and DME cause the exergy loss increase of 8%, 1%, and 4% in MT compared to diesel, respectively.

3.5 Operational costs

The operational cost of the combustor in the MT is analyzed here assuming that the refined and purified biofuels are used, and no extra costs including erosion and corrosions are imposed on the combustor with the use of the different fuels in the combustor. For this combustor, the operational costs are divided into two categories-internal and external costs. The internal costs include the price of the fuel bought from the market. The external cost consists of the price of damages, the fuels have for the environment. Taking these two costs into account, the fiscal advantage of using the MiTREC for the MT is analyzed here. The price of the fuels is considered in US currency $3.55/gallon, $2.35/gallon, $10.5467/thousand cubic feet, and $3.24/gallon for biodiesel, ethanol, NG, and diesel. The price of biogas fuel is considered half of the NG. The price of the emissions CO, CO_2, NO_X are 1.25 US$/L, 0.06 US$/L, 5.09 US$/L, 3.26 US$/L and 0.6 US$/kg, respectively. Other pollutants including HC and SO_X are considered negligible as the combustion efficiency is high and ultra-low Sulphur diesel should be used in MT because of the high sensitivity

of the small MT parts to corrosive materials. The price of fuels and emissions were extracted from International Energy Agency.

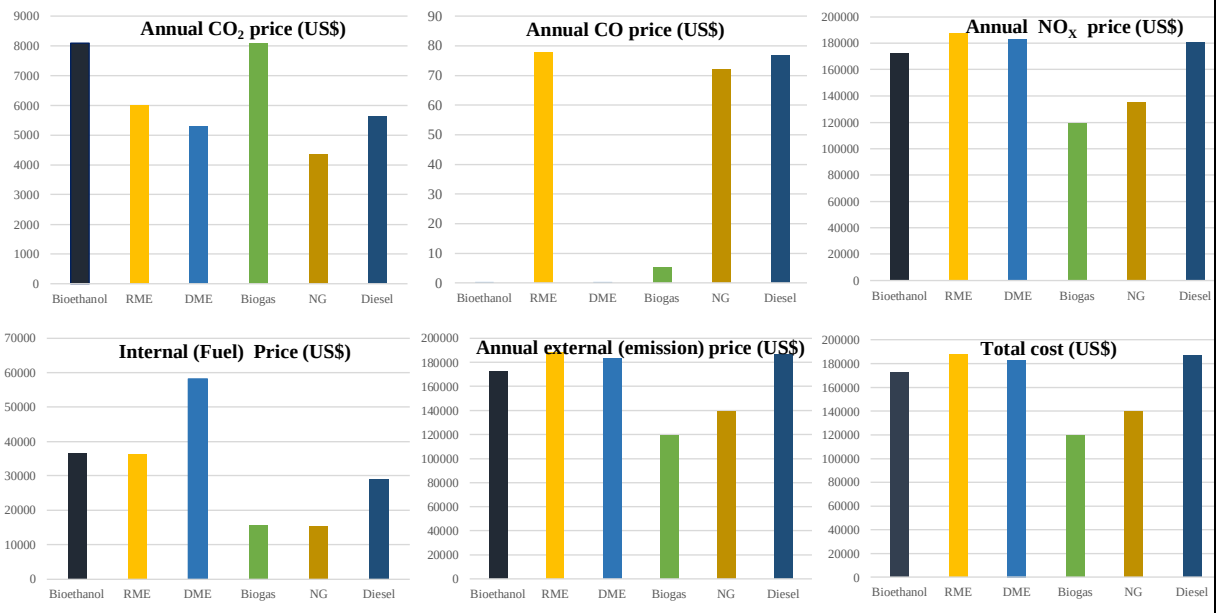

Fig 20 Economical analysis of the MT with the designed combustor fueled with biofuels

Fig 20 depicts the economic analysis of the combustor in terms of fuel, and emission costs. The annual price of emissions, internal, external and total costs are presented (more description about these prices are in [85–87]). The cost analysis of the combustor has shown that biogas fuel is superior to other renewable and fossil fuels leading to remarkable annual savings in operation of MT. These graphs have shown that using bioethanol, DME, biogas, and NG leads to 7.6%, 2%, 36% and 25% reduction in the annual expense of MT. The use of biodiesel leads to 0.65 increase in total costs of the MT when it is considered instead of petrodiesel. The use of biogas leads to the 15% annual saving in the operation of MT when it replaces NG. In a similar case study, Panatelo et al. [88] have revealed that application of biomass in a 100 kWe micro CHP system results in investment profitability. The maximum investment profitability was obtained for 70% input biomass and 30% input natural gas in their case study for Italy.

4. Conclusion

Based on the design perspectives for 12 kWe microturbine, a new vortex type combustor is designed to successfully operate with a range of biofuels without any need for extra equipment to the existing turbine parts. The new combustor is equipped with two adjustable nozzles for gaseous and liquid renewable fuels, a well-established radial air swirler, liner, casing, and appropriate end nozzle for uniform outlet temperature profile and increasing the pressure. The sizing, dimensions, shape, and types of the combustor instruments are determined and optimized through CFD analysis. The combustor switches the different renewable fuels including biogas, biodiesel, bioethanol, and DME by inputting different nozzles for gas and liquid fuels. After design, manufacturing, testing of the combustor, the CFD models were validated using 32 different operating points for biogas and methane fuel. The combustor performance in terms of combustion efficiency, pressure drop, outlet temperature distribution, gaseous emissions is investigated numerically at the company's desired operating point for the microturbine using CFD model. In addition, the operation of the newly designed combustor in the micro-turbine cycle is analyzed, and significant advantages in terms of MT emissions, economical, energy and exergy are obtained with renewable fuel. It was found that the new combustor leads to the efficient performance of MT with renewable fuels with a significant reduction in the levels of gaseous emissions CO_2, NO_X, and CO. It also results in uniform outlet temperature distribution for all fuels and remarkable exo-economy savings with the operation of the new combustor in the MT.

Acknowledgments

The Mirco-Turbine Renewable Energy Combustor (MiTREC Project) is funded by INNOVATE UK under grant number: 103502, as part of the Energy Catalyst Programme for Mid-stage Technology Development to accelerate innovation in the energy sector. The authors greatly

874 acknowledge the help and support of Bladon Micro Turbines members, staff, and management
875 team.

876 5. References

877 [1] Benato A, Stoppato A, Mirandola A, Del Medico M. Design and Off-Design Analysis of an
878 ORC Coupled with a Micro-Gas Turbine. Energy Procedia, 2017.
879 doi:10.1016/j.egypro.2017.09.192.
880 [2] Talluri L, Fiaschi D, Neri G, Ciappi L. Design and optimization of a Tesla turbine for ORC
881 applications. Appl Energy 2018. doi:10.1016/j.apenergy.2018.05.057.
882 [3] McDonald CF, Wilson DG. The utilization of recuperated and regenerated engine cycles for
883 high-efficiency gas turbines in the 21st century. Appl Therm Eng 1996.
884 [4] Udomsri S, Martin AR, Martin V. Thermally driven cooling coupled with municipal solid
885 waste-fired power plant: Application of combined heat, cooling and power in tropical urban areas.
886 Appl Energy 2011. doi:10.1016/j.apenergy.2010.12.020.
887 [5] Lieuwen T, McDonell V, Petersen E, Santavicca D. Fuel flexibility influences on premixed
888 combustor blowout, flashback, autoignition, and stability. Proc. ASME Turbo Expo, 2006.
889 doi:10.1115/GT2006-90770.
890 [6] Ferguson D, Richard GA, Straub D. Fuel interchangeability for lean premixed combustion in
891 gas turbine engines. Proc. ASME Turbo Expo, 2008. doi:10.1115/GT2008-51261.
892 [7] Bazooyar B, Darabkhani HG. Design and numerical analysis of a 3 kWe flameless
893 microturbine combustor for hydrogen fuel. Int J Hydrogen Energy 2019;44:11134–44.
894 doi:10.1016/j.ijhydene.2019.02.132.
895 [8] Al-attab KA, Zainal ZA. Design and performance of a pressurized cyclone combustor (PCC)
896 for high and low heating value gas combustion. Appl Energy 2011.
897 doi:10.1016/j.apenergy.2010.10.041.
898 [9] Li Z, Zou Z, Yao L, Fu C, Bian L, Zhang W. Aerodynamic design method of micro-scale radial
899 turbines considering the effect of wall heat transfer. Appl Therm Eng 2018.
900 doi:10.1016/j.applthermaleng.2018.04.051.
901 [10] Kim MJ, Kim JH, Kim TS. The effects of internal leakage on the performance of a micro gas
902 turbine. Appl Energy 2018. doi:10.1016/j.apenergy.2017.12.029.
903 [11] Bazooyar B, Jomekian A, Karimi-Sibaki E, Habibi M, Gohari Darabkhani H. The role of heat
904 recirculation and flame stabilization in the formation of NOX in a thermo-photovoltaic micro-
905 combustor step wall. Int J Hydrogen Energy 2019. doi:10.1016/j.ijhydene.2019.08.061.
906 [12] Chaudry M, Jenkins N, Qadrdan M, Wu J. Combined gas and electricity network expansion
907 planning. Appl Energy 2014. doi:10.1016/j.apenergy.2013.08.071.
908 [13] Olofsson T, Mahlia TMI. Modeling and simulation of the energy use in an occupied
909 residential building in cold climate. Appl Energy 2012. doi:10.1016/j.apenergy.2011.10.002.
910 [14] Harish VSKV, Kumar A. A review on modeling and simulation of building energy systems.
911 Renew Sustain Energy Rev 2016. doi:10.1016/j.rser.2015.12.040.
912 [15] Bazooyar B, Shariati A, Hashemabadi SH. Characterization and Reduction of NO during the
913 Combustion of Biodiesel in a Semi-industrial Boiler. Energy and Fuels 2015.
914 doi:10.1021/acs.energyfuels.5b01529.
915 [16] Datta A, Som SK. Combustion and emission characteristics in a gas turbine combustor at
916 different pressure and swirl conditions. Appl Therm Eng 1999. doi:10.1016/S1359-

4311(98)00102-1.
[17] Yan Y, Dang L, Deng Y, Li J, Zhao J. Experimental study of flow dynamics and fuel spray characteristics in Lean Premixed Prevaporized Combustor. Fuel 2015. doi:10.1016/j.fuel.2014.12.048.
[18] Benarous A, Karmed D, Liazid A, Champion M. Numerical simulation of a turbulent partially premixed flame with inhomogeneous equivalence ratio. Fuel 2014. doi:10.1016/j.fuel.2014.01.069.
[19] Massucco S, Pitto A, Silvestro F. A gas turbine model for studies on distributed generation penetration into distribution networks. IEEE Trans Power Syst 2011. doi:10.1109/TPWRS.2010.2091290.
[20] Merkel E, McKenna R, Fichtner W. Optimisation of the capacity and the dispatch of decentralised micro-CHP systems: A case study for the UK. Appl Energy 2015. doi:10.1016/j.apenergy.2014.11.036.
[21] Bazooyar B, Darabkhani HG. Design procedure and performance analysis of a microturbine combustor working on biogas for power generation. Proc ASME Turbo Expo 2019;4B-2019. doi:10.1115/GT2019-91052.
[22] Ofualagba G. The modeling and simulation of a microturbine generation system. Int J Sci Eng Res 2012. doi:10.1109/CRIS.2010.5617560.
[23] Sallevelt JLHP, Gudde JEP, Pozarlik AK, Brem G. The impact of spray quality on the combustion of a viscous biofuel in a micro gas turbine. Appl Energy 2014. doi:10.1016/j.apenergy.2014.07.030.
[24] Bazooyar B, Ghorbani A, Shariati A. Combustion performance and emissions of petrodiesel and biodiesels based on various vegetable oils in a semi industrial boiler. Fuel 2011;90:3078–92. doi:10.1016/J.FUEL.2011.05.025.
[25] Bazooyar B, Hallajbashi N, Shariati A, Ghorbani A. An investigation of the effect of input air upon combustion performance and emissions of biodiesel and diesel fuel in an experimental boiler. Energy Sources, Part A Recover Util Environ Eff 2014;36:383–92. doi:10.1080/15567036.2010.538810.
[26] Bazooyar B, Shariati A. A comparison of the emission and thermal capacity of methyl ester of corn oil with diesel in an experimental boiler. Energy Sources, Part A Recover Util Environ Eff 2013. doi:10.1080/15567036.2010.527902.
[27] Habib Z, Parthasarathy R, Gollahalli S. Performance and emission characteristics of biofuel in a small-scale gas turbine engine. Appl Energy 2010. doi:10.1016/j.apenergy.2009.10.024.
[28] Allouis C, Amoresano A, Capasso R, Langella G, Niola V, Quaremba G. The impact of biofuel properties on emissions and performances of a micro gas turbine using combustion vibrations detection. Fuel Process Technol 2018. doi:10.1016/j.fuproc.2018.06.003.
[29] Laranci P, Bursi E, Fantozzi F. Numerical analysis of a microturbine combustion chamber modified for biomass derived syngas. Proc. ASME Turbo Expo, 2011. doi:10.1115/GT2011-45551.
[30] Chiong MC, Chong CT, Ng JH, Lam SS, Tran MV, Chong WWF, et al. Liquid biofuels production and emissions performance in gas turbines: A review. Energy Convers Manag 2018. doi:10.1016/j.enconman.2018.07.082.
[31] Enagi II, Al-attab KA, Zainal ZA. Liquid biofuels utilization for gas turbines: A review. Renew Sustain Energy Rev 2018. doi:10.1016/j.rser.2018.03.006.
[32] Enagi II, Al-attab KA, Zainal ZA. Combustion chamber design and performance for micro gas turbine application. Fuel Process Technol 2017. doi:10.1016/j.fuproc.2017.05.037.

[33] Delattin F, Lorenzo G Di, Rizzo S, Bram S, Ruyck J De. Combustion of syngas in a pressurized microturbine-like combustor: Experimental results. Appl Energy 2010. doi:10.1016/j.apenergy.2009.08.046.
[34] Cadorin M, Pinelli M, Vaccari A, Calabria R, Chiariello F, Massoli P, et al. Analysis of a micro gas turbine fed by natural gas and synthesis gas: Test bench and combustor CFD analysis. Proc. ASME Turbo Expo, 2011. doi:10.1115/GT2011-46090.
[35] Waitz IA, Gauba G, Tzeng YS. Combustors for micro-gas turbine engines. J Fluids Eng Trans ASME 1998. doi:10.1115/1.2819633.
[36] McDonald CF, Rodgers C. Small recuperated ceramic microturbine demonstrator concept. Appl Therm Eng 2008. doi:10.1016/j.applthermaleng.2007.01.020.
[37] Fantozzi F, Laranci P, Bianchi M, De Pascale A, Pinelli M, Cadorin M. CFD simulation of a microturbine annular combustion chamber fueled with methane and biomass pyrolysis syngas - Preliminary results. Proc. ASME Turbo Expo, 2009. doi:10.1115/GT2009-60030.
[38] Zhang RC, Hao F, Fan WJ. Combustion and stability characteristics of ultra-compact combustor using cavity for gas turbines. Appl Energy 2018. doi:10.1016/j.apenergy.2018.05.084.
[39] Fan WJ, Yan M, Yi Q, Yang ML. Low NOx emission of rich-burn, quick-mix, lean-burn trapped vortex combustor. Tuijin Jishu/Journal Propuls Technol 2006.
[40] Ezhil Kumar PK, Mishra DP. Numerical investigation of the flow and flame structure in an axisymmetric trapped vortex combustor. Fuel 2012. doi:10.1016/j.fuel.2012.06.056.
[41] Jin Y, Li Y, He X, Zhang J, Jiang B, Wu Z, et al. Experimental investigations on flow field and combustion characteristics of a model trapped vortex combustor. Appl Energy 2014. doi:10.1016/j.apenergy.2014.08.029.
[42] Straub DL, Casleton KH, Lewis RE, Sidwell TG, Maloney DJ, Richards GA. Assessment of rich-burn, quick-mix, lean-burn trapped vortex combustor for stationary gas turbines. J Eng Gas Turbines Power 2005. doi:10.1115/1.1789152.
[43] Li M, He X, Zhao Y, Jin Y, Yao K, Ge Z. Performance enhancement of a trapped-vortex combustor for gas turbine engines using a novel hybrid-atomizer. Appl Energy 2018. doi:10.1016/j.apenergy.2018.02.111.
[44] Tyliszczak A, Boguslawski A, Nowak D. Numerical simulations of combustion process in a gas turbine with a single and multi-point fuel injection system. Appl Energy 2016. doi:10.1016/j.apenergy.2016.04.106.
[45] Bazooyar B, Gohari Darabkhani H. Analysis of flame stabilization to a thermo-photovoltaic micro-combustor step in turbulent premixed hydrogen flame. Fuel 2019;257:115989. doi:10.1016/J.FUEL.2019.115989.
[46] Yousefi A, Birouk M. Investigation of natural gas energy fraction and injection timing on the performance and emissions of a dual-fuel engine with pre-combustion chamber under low engine load. Appl Energy 2017. doi:10.1016/j.apenergy.2016.12.046.
[47] Seljak T, Širok B, Katrašnik T. Advanced fuels for gas turbines: Fuel system corrosion, hot path deposit formation and emissions. Energy Convers Manag 2016. doi:10.1016/j.enconman.2016.03.056.
[48] Šarlej M, Petr P, Hájek J, Stehlík P. Computational support in experimental burner design optimisation. Appl Therm Eng 2007. doi:10.1016/j.applthermaleng.2007.04.020.
[49] Menter FR. Two-equation eddy-viscosity turbulence models for engineering applications. AIAA J 1994. doi:10.2514/3.12149.
[50] Peters N. Laminar diffusion flamelet models in non-premixed turbulent combustion. Prog Energy Combust Sci 1984. doi:10.1016/0360-1285(84)90114-X.

[51] Selçuk N, Kayakol N. Evaluation of discrete ordinales method for radiative transfer in rectangular furnaces. Int J Heat Mass Transf 1997. doi:10.1016/0017-9310(96)00139-1.
[52] Pei Y, Mehl M, Liu W, Lu T, Pitz WJ, Som S. A multicomponent blend as a diesel fuel surrogate for compression ignition engine applications. J Eng Gas Turbines Power 2015. doi:10.1115/1.4030416.
[53] Herbinet O, Pitz WJ, Westbrook CK. Detailed chemical kinetic oxidation mechanism for a biodiesel surrogate. West. States Sect. Inst. Fall Meet. 2007, 2007.
[54] Smith GP, Golden DM, Frenklach M, Moriarty NW, Eiteneer B, Goldenberg M, et al. GRI-Mech 3.0. URL Http//Www Me Berkeley Edu/Gri_mech 2012.
[55] Fischer SL, Dryer FL, Curran HJ. Reaction kinetics of dimethyl ether. I: high-temperature pyrolysis and oxidation in flow reactors. Int J Chem Kinet 2000. doi:10.1002/1097-4601(2000)32:12<713::AID-KIN1>3.0.CO;2-9.
[56] Marinov NM. A detailed chemical kinetic model for high temperature ethanol oxidation. Int J Chem Kinet 1999. doi:10.1002/(sici)1097-4601(1999)31:3<183::aid-kin3>3.0.co;2-x.
[57] Xuan Y, Blanquart G. A flamelet-based a priori analysis on the chemistry tabulation of polycyclic aromatic hydrocarbons in non-premixed flames. Combust Flame 2014. doi:10.1016/j.combustflame.2013.11.022.
[58] Bazooyar B, Jomekian A, Shariati A. Analysis of the Formation and Interaction of Nitrogen Oxides in a Rapeseed Methyl Ester Nonpremixed Turbulent Flame. Energy & Fuels n.d.;31:8708–21. doi:10.1021/acs.energyfuels.7b01278.
[59] De Soete GG. Overall reaction rates of NO and N2 formation from fuel nitrogen. Symp Combust 1975. doi:10.1016/S0082-0784(75)80374-2.
[60] Westenberg AA. Kinetics of NO and CO in Lean, Premixed Hydrocarbon-Air Flames. Combust Sci Technol 1971. doi:10.1080/00102207108952472.
[61] Senecal PK, Schmidt DP, Nouar I, Rutland CJ, Reitz RD, Corradini ML. Modeling high-speed viscous liquid sheet atomization. Int J Multiph Flow 1999. doi:10.1016/S0301-9322(99)00057-9.
[62] Bazooyar B, Shariati A, Hassan Hashemabadi S. Turbulent Non-premixed Combustion of Rapeseed Methyl Ester in a Free Shear Swirl Air Flow. Ind & Eng Chem Res 2016;55:11645–63. doi:10.1021/acs.iecr.6b02500.
[63] Bazooyar B, Ghorbani A, Shariati A. Physical properties of methyl esters made from alkali-based transesterification and conventional diesel fuel. Energy Sources, Part A Recover Util Environ Eff 2015;37. doi:10.1080/15567036.2011.586975.
[64] Wan J, Fan A, Yao H, Liu W. Flame-anchoring mechanisms of a micro cavity-combustor for premixed H2/air flame. Chem Eng J 2015. doi:10.1016/j.cej.2015.04.011.
[65] Jiang D, Yang W, Chua KJ, Ouyang J, Teng J. Effects of H2/CO blend ratio on radiated power of micro combustor/emitter. Appl Therm Eng 2015. doi:10.1016/j.applthermaleng.2015.04.052.
[66] Jiang D, Yang W, Chua KJ, Ouyang J. Thermal performance of micro-combustors with baffles for thermophotovoltaic system. Appl Therm Eng 2013. doi:10.1016/j.applthermaleng.2013.08.044.
[67] Zhang R, Fan W, Shi Q, Tan W. Structural design and performance experiment of a single vortex combustor with single-cavity and air blast atomisers. Aerosp Sci Technol 2014. doi:10.1016/j.ast.2014.08.017.
[68] Zhang RC, Fan WJ, Shi Q, Tan WL. Combustion and emissions characteristics of dual-channel double-vortex combustion for gas turbine engines. Appl Energy 2014;130:314–25. doi:10.1016/j.apenergy.2014.05.059.

[69] Di Mare F, Jones WP, Menzies KR. Large eddy simulation of a model gas turbine combustor. Combust Flame 2004. doi:10.1016/j.combustflame.2004.01.008.
[70] Bartolini CM, Caresana F, Comodi G, Pelagalli L, Renzi M, Vagni S. Application of artificial neural networks to micro gas turbines. Energy Convers Manag 2011. doi:10.1016/j.enconman.2010.08.003.
[71] Gómez MA, Martín R, Chapela S, Porteiro J. Steady CFD combustion modeling for biomass boilers: An application to the study of the exhaust gas recirculation performance. Energy Convers Manag 2019. doi:10.1016/j.enconman.2018.10.052.
[72] Collazo J, Porteiro J, Patiño D, Miguez JL, Granada E, Moran J. Simulation and experimental validation of a methanol burner. Fuel 2009. doi:10.1016/j.fuel.2008.09.003.
[73] Bazooyar B, Ebrahimzadeh E, Jomekian A, Shariati A. NOx formation of biodiesel in utility power plant boilers. part a: Influence of fuel characteristics. Energy and Fuels 2014. doi:10.1021/ef500001g.
[74] Bazooyar B, Hashemabadi SH, Shariati A. NOXformation of biodiesel in utility power plant boilers; Part B. Comparison of NO between biodiesel and petrodiesel. Fuel 2016. doi:10.1016/j.fuel.2016.05.018.
[75] Visser WPJ, Shakariyants S, De Later MTL, Haj Ayed A, Kusterer K. Performance optimization of a 3KW microturbine for CHP applications. Proc. ASME Turbo Expo, 2012. doi:10.1115/GT2012-68686.
[76] Yoon JJ, Lee HS. The study on development of low NOx combustor with lean burn characteristics for 20KW class microturbine. Proc. ASME Turbo Expo 2004, 2004. doi:10.1115/gt2004-53200.
[77] Laranci P, Bidini G, Zampilli M, Fantozzi F, D'alessandro B, Forcella F. Improving lifetime and manufacturability of an RQL combustor for microturbines: Design and numerical validation. Proc. ASME Turbo Expo, 2015. doi:10.1115/GT2015-43543.
[78] Pashchenko D. Thermodynamic equilibrium analysis of combined dry and steam reforming of propane for thermochemical waste-heat recuperation. Int J Hydrogen Energy 2017. doi:10.1016/j.ijhydene.2017.04.284.
[79] Pashchenko D. Energy optimization analysis of a thermochemical exhaust gas recuperation system of a gas turbine unit. Energy Convers Manag 2018. doi:10.1016/j.enconman.2018.06.057.
[80] Liu T, Zhang G, Li Y, Yang Y. Performance analysis of partially recuperative gas turbine combined cycle under off-design conditions. Energy Convers Manag 2018. doi:10.1016/j.enconman.2018.01.075.
[81] Çengel Y a. Thermodynamics: An Engineering Approach. McGraw-Hill 2004.
[82] de Campos GB, Bringhenti C, Traverso A, Tomita JT. Thermoeconomic optimization of organic Rankine bottoming cycles for micro gas turbines. Appl Therm Eng 2020. doi:10.1016/j.applthermaleng.2019.114477.
[83] Feyzi V, Beheshti M, Gharibi Kharaji A. Exergy analysis: A CO2removal plant using a-MDEA as the solvent. Energy 2017;118:77–84. doi:10.1016/j.energy.2016.12.020.
[84] Malinowski L, Lewandowska M. Analytical model-based energy and exergy analysis of a gas microturbine at part-load operation. Appl Therm Eng 2013. doi:10.1016/j.applthermaleng.2013.03.057.
[85] Bazooyar B, Hosseini SY, Moradi Ghoje Begloo S, Shariati A, Hashemabadi SH, Shaahmadi F. Mixed modified Fe2O3-WO3 as new fuel borne catalyst (FBC) for biodiesel fuel. Energy 2018;149:438–53. doi:10.1016/j.energy.2018.02.062.
[86] Bazooyar B, Shariati A, Hashemabadi SH. Economy of a utility boiler power plant fueled

with vegetable oil, biodiesel, petrodiesel and their prevalent blends. Sustain Prod Consum 2015. doi:10.1016/j.spc.2015.06.001.
[87] Ghorbani A, Bazooyar B. Optimization of the combustion of SOME (soybean oil methyl ester), B5, B10, B20 and petrodiesel in a semi industrial boiler. Energy 2012. doi:10.1016/j.energy.2012.06.035.
[88] Pantaleo AM, Camporeale SM, Shah N. Thermo-economic assessment of externally fired micro-gas turbine fired by natural gas and biomass: Applications in Italy. Energy Convers Manag 2013. doi:10.1016/j.enconman.2013.06.017.